Chromatin modifiers in DNA repair and human disease

Helfricht, A.

2

IDENTIFICATION OF EHMT1 AS A CHROMATIN FACTOR THAT NEGATIVELY REGULATES 53BP1 ACCRUAL DURING THE DNA DOUBLE-STRAND BREAK RESPONSE

Angela Helfricht[1], Bram Herpers[2], Erik H. Danen[2],
Bob van de Water[2], Haico van Attikum[1]

[1] Department of Human Genetics; Leiden University Medical Center
[2] Division of Toxicology; Leiden Academic Centre for Drug Research; Leiden University

ABSTRACT

DNA double-strand breaks (DSB) are the most dangerous species of DNA damage and their repair is crucial to preserve genome stability. Upon DSB induction a highly advanced signaling cascade is activated that leads to several DNA damage-associated histone modifications and the recruitment of chromatin remodelers to make the chromatin more accessible for the accrual of DNA repair proteins. However, the immense crosstalk between these dynamic chromatin modifications is so far poorly understood. To identify novel chromatin regulators that are involved in the response to DSBs, we performed a siRNA screen monitoring the early and late response to DSBs by determining the formation of ionizing radiation (IR)-induced γH2AX and 53BP1 foci, respectively. Amongst others, we found the lysine methyltransferase EHMT1 to negatively regulate 53BP1 accrual to foci. We further show that EHMT1 itself is rapidly recruited to DSBs and promotes DSB repair via both major repair pathways, non-homologous end-joining and homologous recombination. EHMT1 targets H3K9 and other proteins for methylation and we propose that these modifications are likely important during the response to DSBs and for the preservation of genome stability. Future research will certainly demonstrate the exact role of EHMT1 in the DSB response.

INTRODUCTION

DNA double-strand breaks (DSBs) occur on a daily basis when both strands of the DNA duplex are broken. This type of lesions is highly toxic to cells and can be induced by various endogenous and exogenous sources. If not repaired accurately, DSBs can cause genome rearrangements or even cell death. Cells respond to DSBs by activating a complex signaling network that coordinates the recruitment of repair proteins, chromatin organization and cell cycle progression in order to provide time for DNA repair in a permissive chromatin environment.

Upon DSB induction, a series of chromatin modifications are initiated with the Ataxia telangiectasia mutated (ATM)-dependent phosphorylation of the histone H2A variant H2AX (termed γH2AX) being among the first. γH2AX in turn recruits Mediator of DNA damage checkpoint protein 1 (MDC1), which binds γH2AX directly through its BRCT (Lukas et al., 2011; Stucki et al., 2005). MDC1 further coordinates DNA damage-induced histone modifications by providing a binding platform for different chromatin modifying enzymes. First, MDC1 recruits the multisubunit chromatin remodeling NuA4 complex including the acetyltransferase TIP60 to sites of DSBs. Upon DSB induction, Histone protein 1 (HP1) is released from the damaged chromatin, 'unmasking' the abundant H3K9me3 mark to which TIP60 binds through its chromodomain. TIP60 then activates ATM and promotes the DSB response by acetylation of histone H4 at lysine (K) 16 (Kaidi and Jackson, 2013; Sun et al., 2009).

Second, the E3 ubiquitin-protein ligase RNF8 binds through its Forkhead-associated domain to phosphorylated MDC1 and initiates an ubiquitylation signaling cascade within the damaged chromatin (Huen et al., 2007; Kolas et al., 2007; Mailand et al., 2007). RNF8 ubiquitylates histone H2A, which recruits a second E3 ubiquitin-protein ligase RNF168 that amplifies the formed ubiquitin conjugates and also induces novel monoubiquitylation on H2AK13 and 15 (Doil et al., 2009; Gatti et al., 2012; Stewart et al., 2009).

Third, MDC1 attracts the histone lysine methyltransferase MMSET to which it binds in an ATM-dependent manner. MMSET, together with the H4K20 monomethyltransferase SETD8, locally increases de novo dimethylation of H4K20 (H4K20me2) at DSB sites (Oda et al., 2010; Pei et al., 2011). These events together contribute to the accumulation of further downstream signaling factors such as Tumor suppressor p53-binding protein 1 (53BP1), which directly binds as bivalent histone modification reader to ubiquitylated H2AK15 via its ubiquitylation-dependent recruitment motif (Doil et al., 2009; Fradet-Turcotte et al., 2013; Stewart et al., 2009) and to H4K20me2 via its Tudor domain (Botuyan et al., 2006; Zgheib et al., 2009). 53BP1 binding additionally requires the activity of the histone deacetylases HDAC1/2 to counteract TIP60-induced H4K16ac, since this enables local de novo H4K20me2 formation (Hsiao and Mizzen, 2013; Miller et al., 2010; Tang et al., 2013). Furthermore, the removal of the H4K20me2-binders JMJD2A and L3MBTL1 is necessary to reveal this histone mark for 53BP1 binding (Acs et al., 2011; Lee et al., 2008; Mallette et al., 2012; Min et al., 2007). All these events are highly dynamic and scientists are only beginning to understand the immense crosstalk between these DNA damage-induced histone modifications.

Moreover, the structure and composition of chromatin can also be changed by ATP-dependent chromatin remodeling enzymes such as the ATPases Chromodomain-helicase-DNA-binding protein 4 (CHD4) and SWI/SNF-related matrix-associated actin-dependent regulator of chromatin subfamily A member 5 (SMARCA5/SNF2h). Both ATPases are recruited to DSBs and facilitate the efficient recruitment of RNF168, which leads to effective

ubiquitylation and BRCA1 accrual (Luijsterburg et al., 2012; Smeenk et al., 2013). Considering the incredible multitude of chromatin remodeling events during the DSB response, we expected novel chromatin regulating factors to participate in the signaling of DSBs and set out to identify those. To this end, we performed a high-throughput short interfering RNA (siRNA) screen for regulators of the DSB response by simultaneously monitoring the accrual of γH2AX, happening early during the DSB response, and the accumulation of downstream factor 53BP1 into ionizing radiation (IR)-induced foci, which occurs during the later steps of the response to DSBs. Genome-wide screens with a comparable read-out have been performed before (Doil et al., 2009; Paulsen et al., 2009), however so far did not lead to the identification of chromatin modifiers. Moreover, such screens often miss hits for instance due to less strong effects on the read-out. We therefore performed this dedicated high-content microscopy siRNA screen. Amongst others, we identified the histone Eurchromatic histone-lysine N-methyltranferase 1 (EHMT1), also named GLP, as a negative regulator of 53BP1 recruitment into IR-induced foci, while the formation of γH2AX was not affected in EHMT1 knockdown cells. Interestingly, we revealed that EHMT1 is rapidly recruited and promotes DSB repair via both major pathways, non-homologous end-joining (NHEJ) and homologous recombination (HR). Our results thus suggest a role for EHMT1 within the DSB response and EHMT1 is therefore an interesting and novel candidate for maintaining genome stability.

RESULTS

siRNA screen identifies novel chromatin regulators involved in the DSB response

In order to identify novel chromatin regulators involved in the response to DSBs, we carried out a siRNA screen using the Dhamacon Epigenetics SMARTpool library complemented with a custom made SMARTpool library comprising epigenetic modifiers containing a chromo-, bromo- or SANT domain, as well as SNF2-related genes (Table S1A). U2OS cells were reversely transfected with siRNA SMARTpools spotted in 96 well plates and after three days of cultivation, the cells were exposed to 2 Gy of IR. Subsequently, one hour later the cells were fixed and co-immunostained for γH2AX and 53BP1, which was followed by high-throughput confocal imaging. As a read-out the average number of γH2AX and 53BP1 foci/nucleus was determined in duplicate upon knockdown of all 227 targets. To control for siRNA transfection efficiency, we included a siRNA SMARTpool directed against the essential KIF11 gene in each plate, whose knockdown induces cell killing by generating mitotic spindle catastrophes (Weil et al., 2002). Indeed, the knockdown of KIF11 resulted in a ~ 90% reduction in cell viability (Fig. S1). Further controls per plate included siRNAs directed against Luciferase (Luc, negative control) and RNF8 (positive control). The latter is essential for 53BP1 accumulation, but not for γH2AX formation (Doil et al., 2009; Huen et al., 2007; Kolas et al., 2007; Mailand et al., 2007; Stewart et al., 2009). To provide an estimate of the variation within each 96-well plate, these control siRNAs were spotted three times on different locations on each plate. Next, the average numbers of 53BP1 foci of the negative and positive controls per location on the plate were used to calculate the Z-factor. This quality readout was performed for all plates and each time positively met the selection criteria [0.5 < Z-factor < 1] (data not shown). Hence, transfection variation within one 96-well plate did not vary strongly.

To exclude possible knockdown-induced cell growth defects a minimum of 100

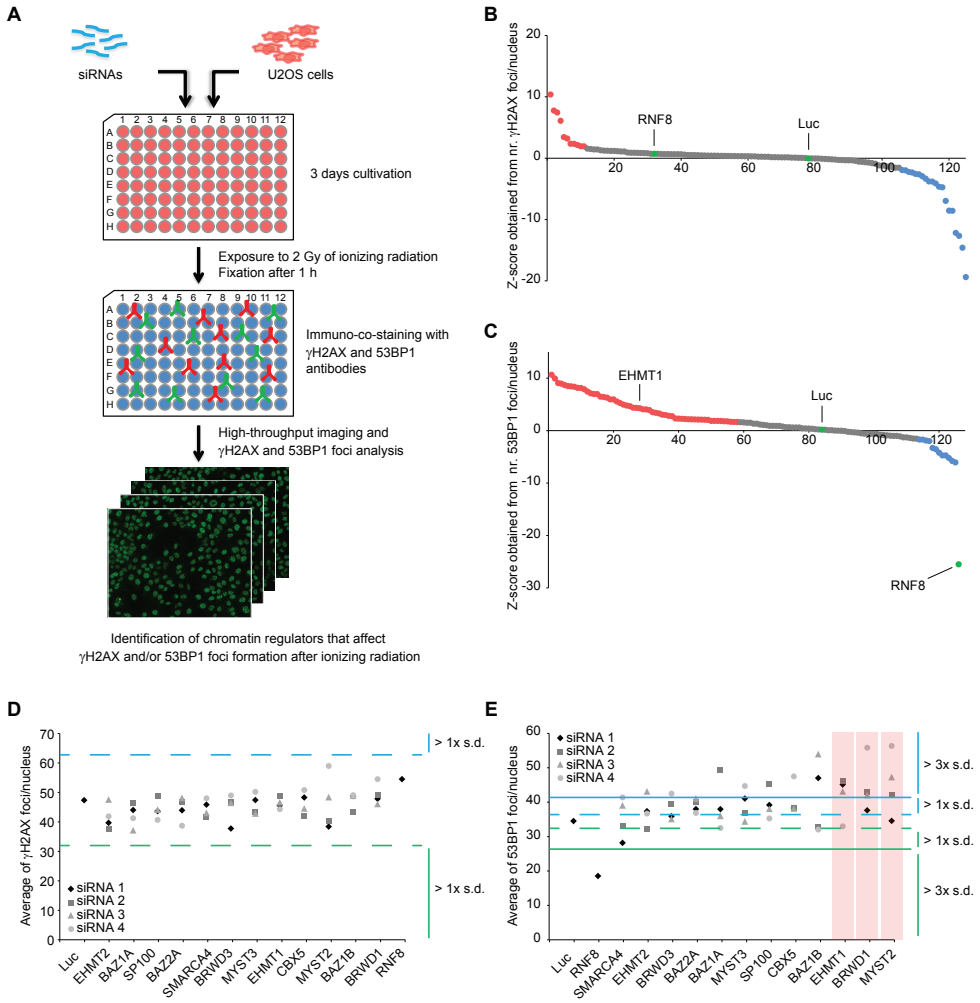

Figure 1. RNAi screen identifies EHMT1 as a regulator of 53BP1 accumulation to DSBs. (A) Schematic of siRNA screen performed to identify novel chromatin regulators involved in the DDR. (B and C) Scatter plot of 124 Z-scores derived from the siRNA screen for γH2AX (B) and 53BP1 (C) foci formation using siRNA Smartpools. Luciferase and RNF8 are indicated as negative and positive control, respectively, for 53BP1 foci formation. The knockdown of targets depicted in red lead to an increase in foci formation, while the depletion of targets shown in blue was followed by a decrease in foci formation. (D and E) Results from secondary validation screen, where four individual siRNAs per target were used to validate the first 12 hits from the primary screen (as in B and C). Shown is the average number of γH2AX (D) and 53BP1 (E) foci/nucleus per siRNA per target from duplicate experiments. One and three times the standard deviation (s.d.) of the Luciferase control are indicated by dashed and continuous horizontal lines, respectively, in blue for an increase and in green for a decrease in average number of foci/nucleus. Confirmed hits are indicated in red where 3 out of 4 siRNAs caused a change in the average foci number/nucleus larger than three times the s.d. of Luciferase. Data of additional 36 hits is presented in Fig. S1.

cells per well were imaged and examined in each of two independent experiments. This criteria was not met for 106 siRNA SMARTpools and led to their exclusion from the dataset (Table S1A). Next, Z-scores were calculated from the average amount of foci per nucleus for each siRNA within one 96-well plate using the siLuc and siRNF8 controls as a reference. The average Z-score from the experimental duplicates provided a measure for the change

in the amount of foci per nucleus upon siRNA treatment compared to control. As expected, depletion of RNF8 caused a dramatic drop in the number of 53BP1 IR-induced foci on each plate (Fig. 1C,E; Fig. S2B,D,F; Table S1A). The knockdown of 32 genes showed a significant effect on γH2AX foci formation, while the depletion of 70 genes by SMARTPpools changed the average amount of 53BP1 foci per nucleus considerably, all meeting the selection criteria [Z-score < -1,5 or > 1,5 and p-value < 0,05] (Fig. 1B,C, Table S1A).

To validate the obtained hit list, we performed a deconvolution screen for which 48 targets were selected, that had been identified in other screens before, but had not yet been functionally characterized (Chou et al., 2010; Hurov et al., 2010; Matic et al., 2010; Matsuoka et al., 2007; Paulsen et al., 2009). For this deconvolution screen we employed four individual siRNAs per target within the same experimental set-up as described above (Fig. 1A,D,E; Table S1B). Here, the average number of foci per nucleus was determined directly from the obtained average foci numbers per nucleus after siRNA treatment from two individual experiments. A gene was considered a hit when at least three out of four siRNAs showed a difference in foci formation larger than three times the standard deviation (s.d.) of the siLuc control. This approach provided more stringent selection criteria for the identification of hits than the thresholds applied in the initial siRNA screen, reducing the chance of obtaining false-positives. Summarizing our results, SDS3 knockdown lead to a decrease in γH2AX foci formation upon IR with all four siRNAs (Fig. S2E; Table S1B), while EHMT1, BRWD1 or MYST2 depletion caused an increase in 53BP1 foci formation after exposure to IR with three distinct siRNAs (Fig. 1D,E; Table S1B).

EHMT1 regulates 53BP1 recruitment into foci

To define whether the siRNA screen approach indeed identified novel factors involved in the DDR, we focused on the histone-lysine N-methyltransferase 1 (EHMT1, also named GLP). EHMT1 is a closely related paralog of EHMT2 (also G9a), both being mammalian lysine methyltransferases (KMTs) that mainly facilitate H3K9 mono- and dimethylation (H3K9me1/2) in euchromatin as well as the methylation of non-histone substrates. Although EHMT1 and EHMT2 can form homomeric complexes, they predominantly exist in a heteromeric complex formed via the interaction of their SET domains (Shinkai and Tachibana, 2011; Tachibana et al., 2005). Observed phenotypes were surprisingly identical in either EHMT1- or EHMT2-deficient mice with embryonic lethality around embryonic day 9.5. Moreover, both EHMT1 and EHMT2 knockout mouse ES cells show a clear reduction in global H3K9me1/2 levels (Tachibana et al., 2002; Tachibana et al., 2005). Importantly, no additive effect was measured in double knockout ES cells, indicating a cooperative rather than a redundant function of these enzymes, and thus an equally important role in the maintenance of H3K9me1/2 throughout chromatin (Tachibana et al., 2005; Tachibana et al., 2008). Interestingly, while mouse Ehmt2 has been shown to be unstable in Ehmt1-/- cells, Ehmt2-/- cells do not show a difference in Ehmt1 protein stability (Tachibana et al., 2005). And while EHMT2 has been shown to interact with a series of DNA-binding and transcriptional repressor proteins such as the DNA methylases DNMT1, DNMT3A and DNMT3B, as well as histone protein 1 (HP1) (Epsztejn-Litman et al., 2008; Shinkai and Tachibana, 2011), a subset of EHMT1 and EHMT2 was found in a multimeric complex together with other histone KMTs such as SUV39H and SETDB1, which can facilitate di- and trimethylation of H3K9 (Fritsch et al., 2010). Upon depositioning of H3K9me1/2 by the EHMT1/2 complex in euchromatin, a repressive chromatin state is induced that forms a substrate for trimethylation by SUV39H at heterochromatic regions as well as for HP1 binding (Bannister et al., 2001; Lachner et al.,

2001; Rice et al., 2003), which leads to heterochromatin formation. Furthermore, EHMT1 function has been suggested to play an important role during neuronal development since loss of function mutations in the EHMT1 gene or submicroscopic deletions of the distal long chromosome arm 9q lead to haploinsufficiency of EHMT1 causing Kleefstra syndrome (KS) (previously 9q subtelomeric deletion syndrome). KS-patients mainly display intellectual disability, childhood hypotonia and characteristic facial anomalies (Kleefstra et al., 1993; Kleefstra et al., 2012; Nillesen et al., 2011). Finally, EHMT1 as well as EHMT2 have been found to be overexpressed in various cancers (Guan et al., 2014; Huang et al., 2010). Concerning these phenotypes and the detected increase in 53BP1 foci formation upon IR exposure in our siRNA screen, we started a follow-up study addressing the role of EHMT1 during the response to DSBs. First, we used two siRNAs against EHMT1 which reduced 53BP1 focus formation in the deconvolution screen to forwardly transfect U2OS cells on 18

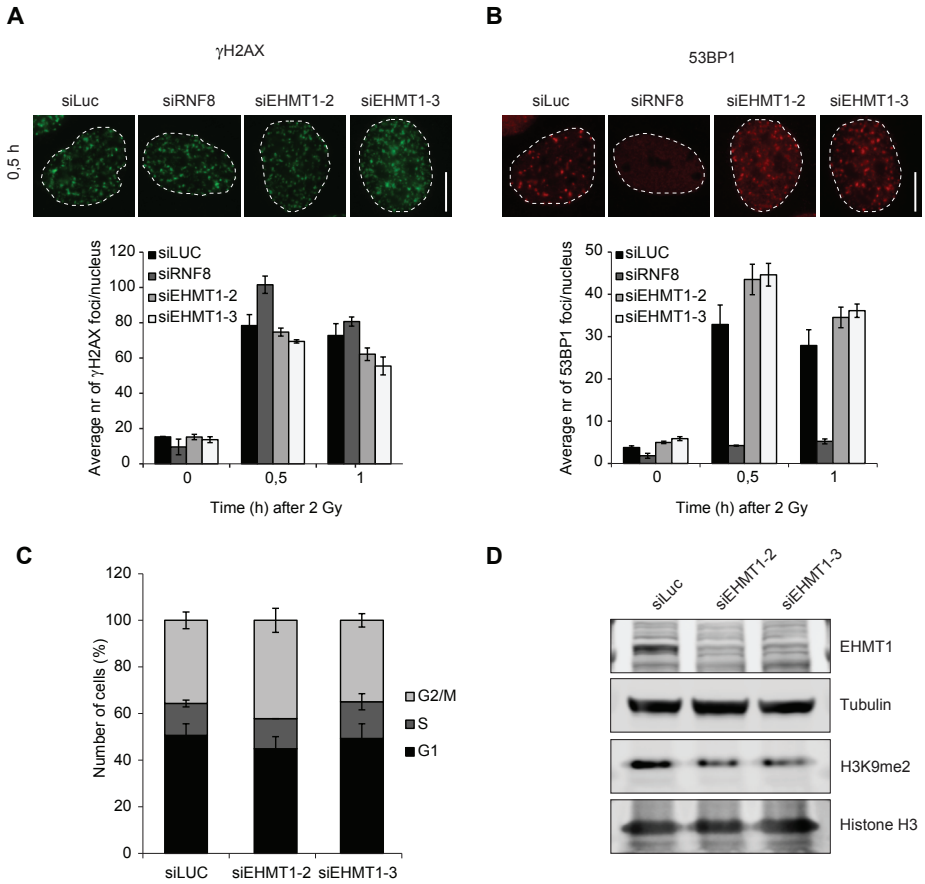

Figure 2. Depletion of EHMT1 leads to an increase in 53BP1 foci formation upon ionizing radiation (IR). (A) U2OS cells were treated with the indicated siRNAs. 48 hours later cells were either left untreated or were exposed to 2 Gy of IR. Cells were immunostained for γH2AX 1 h later. Representative images are shown of the 0,5 h time point. Quantification is depicted using the average number (nr) of γH2AX foci/nucleus obtained from 3 individual experiments where at least 75 cells were examined. Scale bar, 10 µm. (B) As in (A), but immunostained for 53BP1. (C) U2OS cells were transfected with indicated siRNAs and were stained with propidium iodide 48 h later. Cells were then subjected to flow cytometry analysis. Shown is the percentage of cells in G1 (black), S (dark gray) and G2/M phase (light gray). (D) Whole cell extracts from cells in (A) and (B) were subjected to western blot analysis.

mm coverslips and 48 h later, exposed cells to 2 Gy of IR. We determined γH2AX and 53BP1 foci formation after 0.5 and 1 h and again confirmed the increase in 53BP1 foci formation after IR, while depletion of RNF8 showed the expected decrease in 53BP1 recruitment (Fig. 2A,B) (Lukas et al., 2011). To exclude that this effect might indirectly be caused by cell cycle progression defects induced through EHMT1 depletion, we determined the percentage of U2OS cells present in G1, S and G2/M phase in control or EHMT1 knockdown cells. We did not detect a significant difference in cell cycle distribution after EHMT1 deletion, which was confirmed by western blot analysis (Fig. 2C,D). However, we did observe a partial decrease in H3K9me2 upon EHMT1 knockdown (Fig. 2D), which is in agreement with other reports (Chase and Sharma, 2013; Tachibana et al., 2005).

EHMT1 is rapidly recruited to DNA DSBs

Having identified EHMT1 as a novel factor that controls 53BP1 recruitment during the DSB response, we wondered whether EHMT1 itself is recruited to sites of DNA damage.

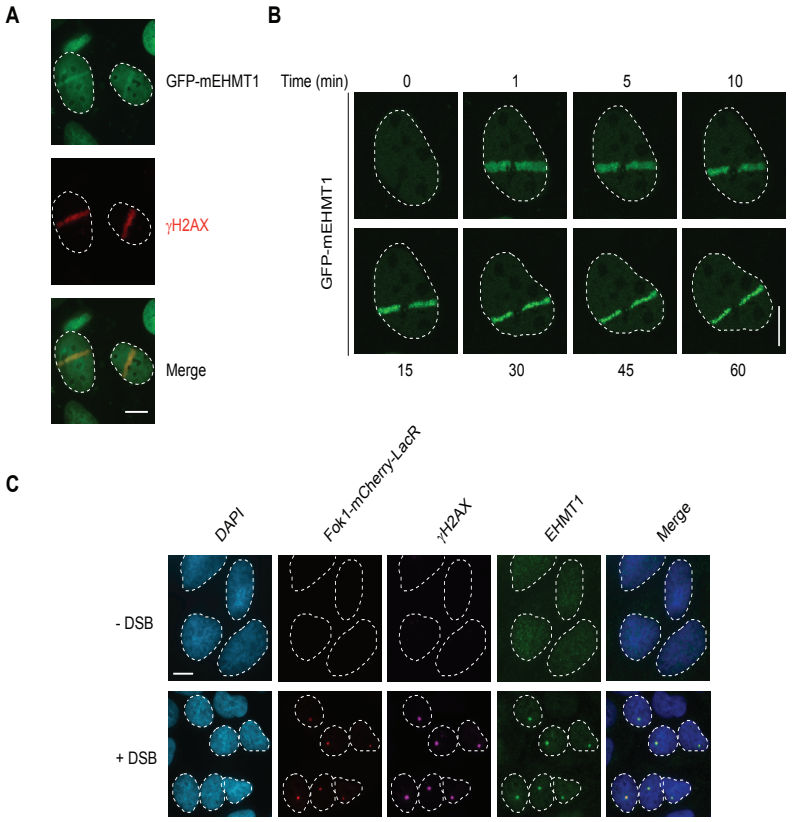

Figure 3. EHMT1 is rapidly recruited to DNA double-strand breaks decorated with γH2AX. (A) GFP-tagged mouse EHMT1 was expressed in U2OS cells which were subsequently subjected to laser micro-irradiation. After 10 min, cells were fixed and immunostained for γH2AX. EHMT1 co-localizes with γH2AX at DNA damage. (B) GFP-mEHMT1 recruitment to laser-induced DNA damage in cells from (A) was monitored in time. Representative images of EHMT1 recruitment of one cell at indicated time points are shown. (C) Immunostaining for γH2AX and EHMT1 at either no or FokI-induced DSBs, which was tagged with mCherry-LacR and re-located to a 200x integrated Lac operator genomic array in U2OS 263 ER-TA cells upon addition of Shield and 4-hydroxytamoxifen 6 h prior to fixation for translocation of FokI-fusion to the nucleus. Scale bars, 10 µm.

Therefore, we locally introduced DNA damage with a Multi-photon (MP) laser in U2OS cells transiently expressing GFP-tagged mouse EHMT1 (Ehmt1), since mouse and human EHMT1 are highly conserved (Fig. S3). Ehmt1 rapidly localized to DSB-containing laser tracks, that were decorated with the DNA damage marker γH2AX (Fig. 3A, B). Ehmt1 was detected already within 1 min after irradiation and remained associated with the damaged chromatin until at least 1 h after laser-mediated DNA damage induction (Fig. 3B). However, since MP laser-irradiation can induce several different types of DNA damage, we employed U2OS 2-6-3 cells to study whether EHMT1 is recruited to site-specific DSBs. Those cells contain an array of lactose operator (LacO) repeats and express instable FokI nuclease fused to the red fluorescent mCherry protein and the E. coli lactose repressor (LacR) (Fig. 3C) (Shanbhag et al., 2010). Upon translocation of the fusion protein to the nucleus mediated via 4-Hydroxytamoxifen and addition of the ligand Shield-1 for Fok1- stabilization, the LacR-fusion protein got targeted to the LacO array, where Fok1 subsequently induced DSBs. Cells were fixed and co-immunostained for γH2AX and EHMT1. Remarkably, endogenous EHMT1 clearly co-localized with Fok1-mCherry-LacR at bona fide DSBs marked by γH2AX. Taken together, these observations confirm the recruitment of EHMT1 to site-specific DSBs, where it somehow regulates the amount of 53BP1 assembly.

EHMT1 promotes DSB repair via Non-homologous end joining (NHEJ) and Homologous Recombination (HR)

In mammals, two major pathways have evolved to repair DSBs. The main pathway is called Non-homologous end-joining (NHEJ) and simply re-ligates the broken DNA ends back together throughout the whole cell-cycle, which can either happen in an error-free or error-prone fashion. The second repair pathway is termed homologous recombination (HR). The functioning of this pathway is restricted to S or G2-phase due to the requirement of a homologous or highly identical template, which is often provided by the sister chromatid (Chapman et al., 2012). To investigate whether EHMT1 contributes to DSB repair, we made use of two well-established reporter assays to monitor DSB repair efficiency in EHMT1-depleted Hek293T cells. The EJ5-GFP NHEJ reporter consists of a GFP gene, which is parted from its promoter due to an insertion of a Puromycine gene that is flanked by two I-SceI recognition sites. DSBs are induced upon transient expression of the rare-cutting I-SceI endonuclease and subsequent excision of the Puromycine gene. Repair of the broken DNA-ends via NHEJ fuses the promoter to the GFP gene and restores GFP expression, which can be measured by flow cytometry (Fig. 4A) (Bennardo et al., 2008). On the other hand, we employed the DR-GFP reporter to study HR, which consists of two differentially mutated GFP genes that are oriented as direct repeats. The upstream repeat carries an I-SceI restriction site, which inactivates gene function, whereas the downstream repeat is a 5' and 3' truncated version of the GFP gene. Transient expression of I-SceI leads to the induction of a DSB in the upstream GFP repeat, which can be repaired by HR using the downstream partial GFP sequence as a homologous template. This leads to the restoration of the GFP gene and consequently to GFP expression detectable by flow cytometry (Fig. 4C) (Weinstock et al., 2006). As expected, depletion of RNF8 and BRCA2 lead to a severe reduction in NHEJ and HR efficiency, respectively (Hu et al., 2014; Roy et al., 2012). Surprisingly, upon depletion of EHMT1 with three different siRNAs, the repair of DSBs via NHEJ as well as HR was considerably reduced (Fig. 4B,D). The knockdown of EHMT1 in Hek293T reporter cells (Fig. 4E) did not cause major changes in cell cycle distribution (Fig. 4F), suggesting that the observed effects were not indirect. The amount of EHMT1-depleted cells in G2/S-phase

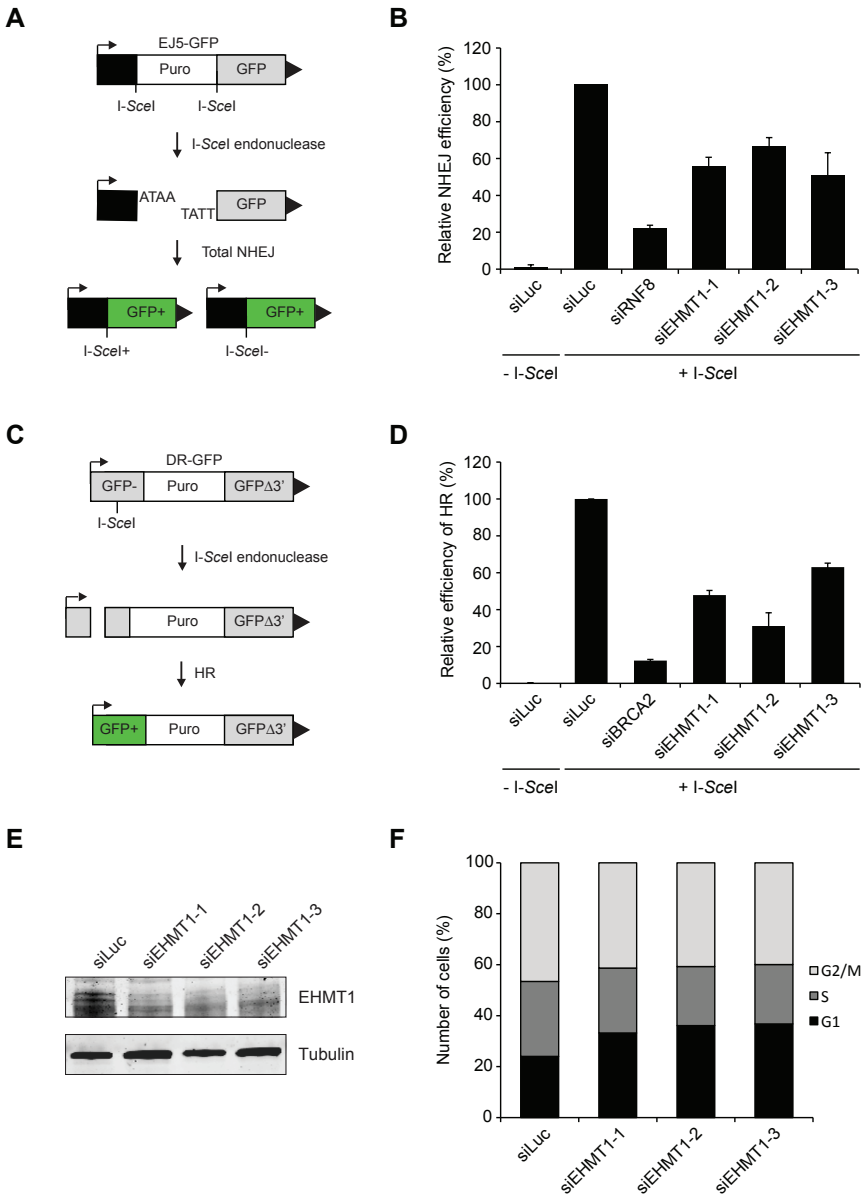

Figure 4. EHMT1 promotes the repair of DSBs via Non-homologous end joining (NHEJ) and Homologous Recombination (HR). (A) Schematic of the EJ5-GFP reporter used to monitor NHEJ efficiency in Hek293T cells (see text for details). (B) EJ5-GFP reporter cells were transfected with the indicated siRNAs. 48 hours later, cells were transfected with a control- or I-SceI expression vector (pCBASce). After additional 48 hours, cells were analysed for GFP expression by flow cytometry. The average of 2 experiments +/- s.e.m. is presented. (C) Schematic of the DR-GFP reporter exploited to investigate HR efficiency in Hek293T cells (see text for details). (D) DR-GFP reporter cells were treated the same way as described in (B). The average of 2 experiments +/- s.e.m. is shown. (E) Hek293T DR-GFP reporter cells were transfected with the indicated siRNAs, followed by transfection with the I-SceI expression vector 48 h later. Cells were stained with propidium iodide 24 h after that and subjected to flow cytometry analysis. The percentage of cells in G1 (black), S (dark gray) and G2/M (light gray) phase is shown. (F) Whole cell extracts from cells in (E) were subjected to western blot analysis.

might have been slightly less when compared to control cells, however it is unlikely that this small difference did cause the considerable drop in DSB repair efficiency upon EHMT1 knockdown. Therefore, these results suggest that EHMT1 promotes the effective repair of DSBs via NHEJ and HR.

DISCUSSION

Major cross-talk exists between histone modifications facilitating a permissive chromatin state in the vicinity of DSBs to promote their signaling and repair as part of the DSB response. In order to gain a better understanding of the spatio-temporal organisation of these chromatin modifications and to identify novel chromatin regulators with a role in the DSB response, we performed an siRNA-based high-throughput microscopy screen. With this approach we found the lysine methyltransferase (KTM) EHMT1 amongst several other hits to negatively regulate 53BP1 foci formation. Additionally, we showed that EHMT1 is rapidly recruitment to DSBs and that it promotes DSB repair via both major repair pathways, NHEJ and HR. EHMT1 thus is a novel candidate for the maintenance of genome stability.

siRNA Screen for novel chromatin regulators

By examining γH2AX or 53BP1 foci formation upon IR, we could monitor the early and late events during the response to DSBs. Hence, we not only gathered information about novel chromatin regulators and whether or not they have a role during the DDR, but could also define their moment of action more closely. 53BP1 thereby was a suitable read-out candidate to screen for, as several distinct chromatin modifications are required for and contribute to its accrual at DSBs.

We obtained a long list of possible chromatin regulators affecting either γH2AX and/or 53BP1 accrual to IR-induced foci from the primary screen. Among those hits, known regulators of γH2AX were found such as BAZ1B (WSTF), which is involved in the global phosphorylation of H2AX on Y142 (Xiao et al., 2009), a mark that needs to be removed upon damage induction for proper MDC1-binding to γH2AX at S139 (Cook et al., 2009; Krishnan et al., 2009). Moreover, depletion of the ATP-dependent chromatin remodeler SMARCA4 (BRG1) led to a decrease in γH2AX foci formation. This is in agreement with recent reports, which indicated that SMARCA4 is phosphorylated by ATM upon DSB induction and promotes γH2AX formation as well as DSB repair through the binding of acetylated histone H3 in γH2AX-containing nucleosomes (Kwon et al., 2015) (Table S1A). We further detected an increase in 53BP1 foci formation after IR in cells depleted from JMJD2A, which has been shown to mask H4K20me2, subsequently preventing 53BP1 binding at DSBs. For 53BP1 binding to occur, JMJD2A needs to be targeted for degradation through ubiquitylation by RNF168 upon DSB induction (Lee et al., 2008; Mallette et al., 2012). Likewise, the depletion of CBX5, better known as HP1α, was found to cause elevated levels of 53BP1 foci, which is in agreement with previously published results (Lee et al., 2013).

With a selection of 48 hits from this primary screen, a deconvolution screen was performed. We were able to confirmed 4 hits, of which we selected EHMT1 for a follow-up study. Its regulatory effect on 53BP1 accrual to DSBs was successfully validated during a second IR-induced foci experiment, where another format and different siRNA transfection method was used (Fig. 2A,B). This thus shows the ability of our screening approach to identify novel factors involved in the DSB response. However, potential hits might also

have been missed out on due to knockdown efficiency issues, since we could not control siRNA transfection efficiency per individual siRNA. Nonetheless, siKIF11 transfection led to 90% cell death and a strong decrease in 53BP1 foci formation was observed upon RNF8 depletion. Hence, the controls for siRNA transfection efficiency indicated the effectiveness of the applied transfection protocol. Additionally, the reproducibility of the generated data was confirmed by the calculation of the Z-factor for each plate, that all met the threshold criteria.

Stringent selection during deconvolution screen

Due to the biased target selection of epigenetic regulators and the high number of possible hits obtained from the primary screen, we stringently applied thresholds during the analysis of the deconvolution screen. Here, 3x the standard deviation of the siLuc control was used as selection criteria, which led to the confirmation of EHMT1 as a hit, but excluded its related heterodimer-partner EHMT2 from the hit list (Table 1B) (Tachibana et al., 2005). Interestingly, EHMT2 would have been a hit under the threshold of 1x the standard deviation (Fig. 1E; Table S1A,B). This less pronounced increase in 53BP1 foci formation in EHMT2-depleted cells could have been caused by insufficient siRNA transfection efficiency. On the other hand, this could also hint towards an independent function of EHMT1 in the response to DSBs. However, the H3K9 mono- and dimethylation activities were assigned to both KMTs and loss of one or the other leads do a clear decrease in global H3K9me1/2 levels (Tachibana et al., 2005; Tachibana et al., 2008). Subsequently, further verification of the role of EHMT2 in the DSB response either dependent or independent of EHMT1 is therefore required.

EHMT1 recruitment to DSBs

Although EHMT1 was identified as a negative regulator of 53BP1 accrual into IR-induced foci, we found that γH2AX formation remained unaffected in EHMT1-depleted cells (Fig. 1D,E; Table S1A,B). This suggests that the activity of EHMT1 is important for the more downstream steps of the DSB response. However, EHMT1 is recruited rather rapidly to DSBs (Fig. 3), which might hint towards a role in a process taking place immediately after DNA damage induction, yet one that controls 53BP1 recruitment. To further categorize EHMT1 into the numerous events of the DDR, the recruitment of other important DSB response factors such as MDC1, RNF8 or RNF168 to IR-induced foci or laser-induced DNA damage should be monitored in the absence of EHMT1. Moreover, the recruitment of several DSB response factors is highly dependent on the phosphorylation activity of ATM on serine (S) target sites. Both, EHMT1 and EHMT2, have shown to contain ATM-/ATR-target sites on Ser466 and Ser569, respectively (Matsuoka et al., 2007). It is therefore likely, that EHMT1 and EHMT2 are recruited in an ATM-dependent fashion, but this still requires experimental confirmation. Another way to rapidly recruit EHMT1 could be facilitated through the action of poly(ADP-ribose) polymerase 1 (PARP1), which attaches poly(ADP-ribose) chains onto itself and other target proteins upon DSB induction (Bekker-Jensen and Mailand, 2010; Smeenk et al., 2013). Since the recruitment of the histone tri-methylase SUV39H was found to be PARP-dependent (Ayrapetov et al., 2014), it would be interesting to investigate the contribution of PARP to EHMT1 recruitment in cells depleted from PARP or treated with an PARP inhibitor.

Possible role of EHMT1 at DSBs

Once EHMT1 is recruited to DSBs, it exerts a yet unknown function. However, it has been

generally described to mono- and dimethylate H3K9 within euchromatin, together with EHMT2 (Tachibana et al., 2005). Since di- and trimethylation of H3K9 was shown to locally increase upon DSB induction (Ayrapetov et al., 2014; Khurana et al., 2014), the question arises whether EHMT1/2 contribute to establish H3K9me2 at DSBs. For the binding of oligomerized 53BP1 at DSBs, RNF168-ubiquitylated H2AK15 (Fradet-Turcotte et al., 2013) and H4K20me2, established through the combined action of MMSET and SETD8, are required (Panier et al., 2012). But how could the H3K9 methyltransferase activity of EHMT1 affect 53BP1 accumulation? We hypothesize that it might perform the first two methylation steps on H3K9 upon DSB induction providing the substrate for SUV39H H3K9 trimethylation, which is an important mark for the recruitment and activation of TIP60 to DSBs (Sun et al., 2009). TIP60 binds H3K9me3 and acetylates H4K16 (Hsiao and Mizzen, 2013; Tang et al., 2013), which prevents de novo H4K20 mono- and dimethylation by SETD8 and MMSET (Huen et al., 2008; Pei et al., 2011). However, upon DSB induction the histone deacetylases HDAC1/2 are recruited and facilitate the deacteylation of H4K16 (Miller et al., 2010), paving the way for SETD8 and MMSET and promoting 53BP1 accrual. Other proteins bound to H4K20me2 such as L3MBTL1 and JMJD2A are then removed from chromatin in the vicinity to the DSB by eviction or proteasomal degradation (Acs et al., 2011; Mallette et al., 2012; Meerang et al., 2011). Hypothetically, when translating these events to the case of EHMT1-depletion, H3K9me3 would not be established for TIP60 binding, highly stimulating H4K20 methylation followed by an increase of 53BP1 assembly at DSBs, which describes the exact phenotype obtained during the siRNA screen and validation experiments (Fig. 1E,2B).

To investigate this hypothesis experimentally, one could use ChIP to examine whether a local decrease in H3K9 methylation levels at DSBs can be detected in EHMT1-depleted or -inhibitor treated cells compared to untreated cells. Additionally in a similar set-up, H4K16ac levels could be examined at DSBs looking for a decrease in H4K16ac in cells with no functional EHMT1 like it has been done for SUV39H-depleted cells showing a loss in H4K16-acetylation (Ayrapetov et al., 2014). This would indicate that EHMT1/2-mediated H3K9 methylation is required for TIP60 binding and activity. And since a portion of EHMT1 and EHMT2 was found to form a multimeric complex with SUV39H and the histone di-/trimethyltransferase SETDB1 (Fritsch et al., 2010), the combined action of these histone mono-/di- and trimethylases seems plausible in order to facilitate DSB-dependent local H3K9me3 regulating 53BP1 accrual.

EHMT1 also would not be the first H3K9 dimethyltransferase implicated in the DSB response, since the PR domain zinc finger protein 2 (PRDM2), together with the repressive macrohistone variant macroH2A1, has been shown to promote the formation of condensed chromatin in a manner dependent on ATM and dimethylation of H3K9. These events ultimately facilitate DSB end resection, BRCA1 recruitment and DSB repair via HR (Khurana et al., 2014). Conversely, H3K9me3 has been suggested to only transiently increase following the rapid accumulation of the KAP1/HP1/SUV391H complex to DSBs. Once TIP60 is activated through the binding of the established H3K9me3 mark, it acetylates ATM and H4. This is immediately followed by ATM-dependent KAP1 phosphorylation, which leads to the release of the KAP1/HP1/SUV391H complex from chromatin (Ayrapetov et al., 2014). The authors reasoned that ATM activation functions as negative feedback loop through the removal of repressive SUV39H from DSBs, possibly limiting DSB repair. However, whether KAP1/HP1/SUV39H only induces transient H3K9me3 is questionable, since SET just recently has been shown to be recruited to DSBs, where it interacts with KAP1 and induces the retention of KAP1 and HP1 at DSBs. When overexpressed, a compact chromatin state is established that

limits uncontrolled DSB signaling and inhibits DNA end resection as well as repair via HR during S/G2 phase of the cell cycle (Kalousi et al., 2015). Thus, that H3K9 methylation is strictly regulated during the DSB response to induce repressive chromatin formation either transiently or in general becomes increasingly clear. However, future research is required to define the persistence of H3K9me3 and the role of EHMT1/2 in H3K9me3 establishment at DSBs.

Potential consequences of EHMT1 overexpression

Where the depletion of EHMT1 leads to an increase in 53BP1 recruitment to DSBs, its overexpression might actively abrogate the response to DSBs by promoting H3K9 methylation and simultaneous HP1- or TIP60-binding that subsequently leads to H4K16-acetylation. This would result in a restrained availability of binding sites for 53BP1 at DSBs. When testing this hypothesis experimentally, we observed that transiently overexpressed Ehmt1 is rapidly recruited to DSB-containing laser tracks, where Ehmt1 remained present for at least 1 h at the site of DNA damage (Fig. 3A). Interestingly, upon a more closely investigation of those laser tracks, we could detect a decrease in the spreading of GFP-tagged Ehmt1 within the damaged chromatin compartment over time, which would support the hypothesis that Ehmt1 overexpression negatively regulates the DSB response. However, to map the consequences of EHMT1 overexpression, the track width, which is a measure reflecting the extent to which factors spread into the damaged chromatin compartment, should be determined in time after DNA damage induction by laser micro-irradiation for EHMT1 and 53BP1. If this theory holds, 53BP1 accrual would be clearly decreased and less expanded upon excessive EHMT1 expression. Additional research however needs to point out whether that is the case.

EHMT1 also methylates non-histone targets

EHMT1/2 can methylate itself, H3K9 and, several non-histone proteins. Methylation of the Widely-interspaced zinc finger-containing protein (WIZ) stabilizes EHMT1/EHMT2 complex formation through the binding of its sixth zinc-finger motif to the SET-domains of EHMT1/EHMT2. WIZ thereby acts as an adaptor molecule that stabilizes EHMT2 and might drive the dominant heteromeric complex formation of EHMT1/2 in vivo (Tachibana et al., 2005; Ueda et al., 2006). Hence, WIZ might indirectly be involved in the regulation of 53BP1 levels during the DSB response via the action of the EHMT1/2-WIZ complex. Another established target of EHMT1/2 methylation is the tumor suppressor p53 which is primarily dimethylated on K737. This process in turn is regulated by the E3 ubiquitin ligase MDM2 (Chen et al., 2010; Huang et al., 2010). Upon DSB induction, MDM2 and p53 are phosphorylated by ATM leading to a de- or increase in their protein stability, respectively (Khosravi et al., 1999). However under these conditions, K737me2 levels of p53 remained the same, which indicates that this mark correlates with inactive p53. This is supported by the fact that upon EHMT1/EHMT2-depletion the levels of apoptotic cells increase due to p53 release from K373me2-mediated repression (Huang et al., 2010), something we did observe visually but did not measure in the performed cell-cycle experiments of EHMT1-depelted cells (Fig. 2C,4F). Whether and if so, how the methylation of these and possible unknown targets is related to the role of EHMT1 in regulating 53BP1 levels during the DSB response remains unclear and requires further investigation.

Additionally, EHMT1/EHMT2 targets have been identified by immunoprecipitating methylation target proteins with the GST-tagged methyl-binding domain of L3MBTL1 from

cells treated without or with an inhibitor for EHMT1/EHMT2 (UNC0638). Interestingly, amongst others the DNA repair factors DNA ligase 1 (LIG1), DNA-dependent protein kinase catalytic subunit (DNA-PKcs) and the chromatin remodeler SMARCA5 have been identified as methylation-candidate targets of EHMT1/EHMT2 (Moore et al., 2013). Future studies need to reveal the role of EHMT1/EHMT2-dependent methylation of these factors during the response to DSBs. However, there is also a possibility that EHMT1 might exert a yet unknown function, which is not connected to its described lysine methylation activity. In that case, recruitment studies of DSB response factors would provide insights on the spatio-temporal activity of EHMT1 during the DSB response and would lead to appropriate follow up studies.

EHMT1 is involved in the efficient repair of DSBs via NHEJ and HR

The well-established EJ5-GFP and DR-GFP reporters used to monitor DSB repair efficiency of NHEJ or HR, respectively, clearly suggest a role for EHMT1 during the repair of DSBs (Fig. 4A-D). As previously discussed, EHMT1 seems to regulate 53BP1 accrual, which has been identified as an important factor driving NHEJ by preventing resection at DSBs and the subsequent assembly of HR factors (Panier et al., 2012). However, EHMT1 depletion promotes both repair pathways in the employed reporter assays. To gain a better understanding of how EHMT1 can promote NHEJ as well as HR, a possible additive effect on DSB repair efficiency could be monitored by additional depletion of 53BP1 from siEHMT1 treated DR-GFP reporter cells. Moreover, besides the recruitment of 53BP1 and BRCA1 in siEHMT1 treated cells, the accumulation of DSB signalling factors like RNF8 and RNF168, DNA end resection factors like CtIP and RPA or DSB repair factors like XRCC4 and RAD51 could be monitored to locally laser micro-irradiated regions or IR-induced foci. This would more precisely define EHMT1's mode of action during DSB signalling and repair. Finally, there is also a possibility that EHMT1 exerts diverse, yet unknown functions within the two different repair pathways. In any case, revealing the function of EHMT1 will instantly lead to a better understanding of how it can contribute to the repair of DSBs via both repair pathways.

EHMT1 involved in intellectual disability syndrome and cancer

Loss of function mutations in EHMT1 are one cause of the intellectual disability disorder Kleefstra syndrome in humans (Kleefstra et al., 1993; Kleefstra et al., 2012; Nillesen et al., 2011). This phenotype is also conserved in Drosophila where EHMT-deficiency apparently leads to defects in learning and memory (Kramer et al., 2011). Moreover, EHMT1 and EHMT2 knockout mice are embryonic lethal and global H3K9me1/2 levels are highly reduced in knockout ES cells (Tachibana et al., 2002; Tachibana et al., 2005), indicating an important role for EHMT1/2 activity in mammalian development. Furthermore, EHMT1 and EHMT2 have been reported to be overexpressed in various cancers (Guan et al., 2014; Huang et al., 2010), which suggests a role as putative oncogenes. Consequently, they may form promising anti-cancer drug targets for the development of chemical inhibitors. Encouragingly for such a purpose, EHMT2 knockdown appeared to inhibit tumor cell growth in vitro and induced extensive chromosome instability (Kondo et al., 2008). Consequently, EHMT1- and EHMT2-dependent maintenance of H3K9 methylation in euchromatin and/or methylation of other target proteins such as p53 and mentioned DNA repair factors seems highly important for the preservation of genome stability.

MATERIAL AND METHODS

Cell culture

U2OS cells, U2OS 263 cells containing a 200x integrated Lac operator genomic array and HEK293T cells were grown in DMEM (Gibco) containing 10% FCS (Bodinco BV) and 1% penicillin/streptomycin unless stated otherwise. U2OS 263 cells were a gift from Susan Janicki (Shanbhag et al., 2010) and were grown in the presence of G418 [400 μg/ml].

siRNA screen

siRNAs, from Dharmacon siGENOME® SMARTpool® Epigenetics siRNA library supplemented with 80 custom siGENOME® SMARTpool® siRNAs for the first screen and from a customized library containing sets of four single siRNA per target for the validation screen, were spotted into 96-well glass bottom plates. Additionally, the negative control Luciferase (Luc) and positive controls RNF8 and KIF11 were spotted 3 times at different locations per 96-well screening plate. Reverse siRNA transfection was performed by adding first HiPerFect transfection reagent (QIAGEN) to each well according to manufacturer instructions and secondly U2OS cells in DMEM (Gibco) containing 10% FCS (Bodinco BV). Cells were cultivated at 37°C and after 24 h, media was refreshed with DMEM containing 10% FCS and 1% penicillin/streptomycin. 48 hours later, cells were exposed to 2 Gy of ionizing radiation (IR) and fixed after 1 h at 37°C with 4% formaldehyde for 10 min. Cells were treated with 0.1% Triton X-100 in PBS for 5 min and rinsed with PBS, followed by equilibration of cells in PBS containing 5 g BSA/L and 1.5 g glycine/L prior to immunostaining for γH2AX (1:2000, #07-164, Millipore) and 53BP1 (1:1000, #NB100-304, Novus Biologicals). Detection of primary antibodies was accomplished using goat anti-mouse or goat anti-rabbit IgG coupled to Alexa 488 or 555 (Invitrogen Molecular probes). Cells were incubated with DAPI [0.1 μg/ml] and after several PBS washes kept in PBS at 4°C. High-throughput imaging was performed on a BD pathway equipped with a Nipkow spinning disc for confocal imaging and a 40x objective. Each screen was executed in duplicate and BD Image Data Explorer software version 2.3.1 was used from BD Biosciences for automated analysis to determine the average number of foci/nucleus. Z-scores were calculated from the duplicates per 96-well plate with following formula:

$$Z\text{-score} = (x - \mu) / ó$$

x – raw score,
μ - mean of Luc per plate,
ó – std dev of Luc per plate (Doil et al., 2009).

Z-scores with a cut-off of 1.5 below or above the reference and a p-value lower than 0,05 were categorized as hit in the first screen using SMARTpool® siRNAs. During the validation screen the average amount of foci/nucleus was determined from duplicates employing the set of four single siRNAs per target of which at least three needed to cause a difference of more than 3 times the standard deviation from Luciferase to be assigned as hit.

Transfections and RNAi interference

siRNA and plasmid transfections were performed using Lipofectamine RNAiMAX (Invitrogen) or Lipofectamine 2000 (Invitrogen), respectively, according to the manufacturer's instructions. During the follow-up study, the following siRNA sequences were used:

5’- CGUACGCGGAAUACUUCGA -3’ (Luciferase, Dharmacon),
5’- GAGGGCCAAUGGACAAUUA -3’ (RNF8, Dharmacon),
5’- CAAACAGCGUGGUCAAGUA -3’ (EHMT1-1, Dharmacon),
5’- CAAGAAAGGCCACUACGAA -3’ (EHMT1-2, Dharmacon),
5’- GGAAUUCUGUCUUCACAAG -3’ (EHMT1-3, Dharmacon),
5’- AUAUGUUGGUGAACUGAGA -3’ (XRCC4, Dharmacon),
5’- GAAGAAUGCAGGUUUAAUA - 3’ (BRCA2, Dharmacon).

Cells were transfected twice with siRNAs [40 nM] within 24 h and examined further 48 h after the second transfection unless stated otherwise.

Generation of DSBs
IR was delivered by a YXlon X-ray generator (YXlon International, 200 KV, 4 mA, dose rate 1.1 Gy/min). In U2OS 263 cells, DSBs were induced throughout the addition of Shield [1 μM] (Clontech) and 4-Hydroxytamoxifen [300 nM] to the growth media (Guan et al., 2014; Shanbhag et al., 2010) to induce nuclear expression of the mCherry-LacR-FokI fusion that localizes to the LacO array, where Fok1 induces DSBs (Shanbhag et al., 2010). Cells were subsequently fixed with 4% formaldehyde after 6 h followed by immunostaining.

Plasmid
GFP-mEHMT1 expression vectors were obtained from Yoichi Shinkai (Tachibana et al., 2005).

Laser micro-irradiation
Multiphoton laser micro-irradiation was carried out on a Leica SP5 confocal microscope equipped with an environmental chamber set to 37°C (Helfricht et al., 2013). Briefly, U20S cells were grown on 18 mm glass coverslips and media was replaced with CO2-independent Leibovitz L15 medium, both supplemented with 10% FCS and 1% penicillin/streptomycin. Cells were placed in a Chamlide TC-A live-cell imaging chamber before imaging and were kept at 37°C. DSB-containing tracks (1.5 μm width) were generated with a Mira modelocked Ti:Sapphire laser (λ = 800 nm, pulselength = 200 fs, repetition rate = 76 MHz, output power = 80 mW). Typically, cells were micro-irradiated with 1 iteration per pixel using LAS-AF software, incubated for the indicated time-points at 37°C and subsequently fixed with 4% formaldehyde before immunostaining. For live cell imaging, confocal images were recorded before and after laser irradiation at different time intervals.

Immunofluorescent labelling
Immunofluoresecent labeling of γH2AX and EHMT1 was performed as described previously (Helfricht et al., 2013). Briefly, cells were grown on glass coverslips and treated as indicated in the figure legends. Subsequently, cells were washed with PBS, fixed with 4% formaldehyde for 10 min and treated with 0.1% Triton X-100 in PBS for 5 min. Cells were rinsed with PBS and equilibrated in PBS containing BSA [5 g/l] and glycine [1.5 g/l) prior to immunostaining. Detection was done using goat anti-mouse or goat anti-rabbit IgG coupled to Alexa 488, 555 or 647 (Invitrogen Molecular probes). Samples were incubated with DAPI [0.1 μg/ml] and mounted in Polymount.

Microscopy analysis
Images of fixed samples were acquired on a Zeiss AxioImager M2 widefield fluorescence

microscope equipped with 40×, 63×, and 100× PLAN APO (1.4 NA) oil-immersion objectives (Zeiss) and an HXP 120 metal-halide lamp used for excitation, as well as ZEN software (2012). Fluorescent probes were detected using the following filters: DAPI (excitation filter: 350/50 nm, dichroic mirror: 400 nm, emission filter: 460/50 nm), GFP/Alexa 488 (excitation filter: 470/40 nm, dichroic mirror: 495 nm, emission filter: 525/50 nm), mCherry (excitation filter: 560/40 nm, dichroic mirror: 585 nm, emission filter: 630/75 nm), Alexa 555 (excitation filter: 545/25 nm, dichroic mirror: 565 nm, emission filter: 605/70 nm), Alexa 647 (excitation filter: 640/30 nm, dichroic mirror: 660 nm, emission filter: 690/50 nm). The average number of IR-induced foci per nucleus was determined using ImageJ and the IRIF analysis 3.2 Macro as previously described (Typas et al., 2015).

Cell cycle profiling

For cell cycle analysis cells were fixed in 70% ethanol, followed by DNA staining with 50 μg/ml propidium iodide in the presence of RNase A (0.1 mg/ml). Cell sorting was performed on a BD LSRII flow cytometer (BD Bioscience) using FACSDiva software version 5.0.3. Obtained data was quantified with Flowing software 2.5.1 (by Perttu Terho in collaboration with Turku Bioimaging).

Western blot analysis

Protein extracts were generated by direct lysis of cells in 2x Laemmli buffer and boiled for 10 min at 950C. Proteins were size separated using Novex 4-12% Bis-Tris mini gels (Invitrogen) in 1x MOPS buffer (Invitrogen) and transferred to PVDF membranes, which were blocked in 4% milk for at least 30 minutes and incubated with the indicated antibodies overnight. Several wash steps before and after 1 h incubation with secondary antibodies rabbit-anti-700 and mouse-anti-800 (Sigma) were executed. Protein bands were visualized using the Odyssey infrared imaging system (Licor) according to manufacturer's instructions.

Antibodies

Immunofluorescence and western blot analysis were performed using antibodies against γH2AX (1:1000-2000, #07-164, Millipore), 53BP1 (1:1000, #NB100-304, Novus Biologicals), EHMT1 (1:500, #B0422, R&D Systems), α-Tubulin (1:1000, #T6199 clone DM1A, Sigma), Histone H3K9me2 (1:500, #1220, Abcam) and Histone H3 (1:1000, #1791, Abcam).

Homologous recombination and Non-homologous end-joining repair assay

HEK293 cell lines containing a stably integrated copy of the DR-GFP or EJ5-GFP reporter, respectively, were used to measure the repair of I-SceI-induced DSBs via NHEJ or HR (Bennardo et al., 2008; Pierce and Jasin, 2014; Weinstock et al., 2006). Briefly, 48 h after siRNA transfection, cells were transfected with the I-SceI expression vector pCBASce and a mCherry expression vector (Pierce et al., 1999). 48 h later the fraction of GFP-positive cells among the mCherry-positive cells was determined by FACS on a BD LSRII flow cytometer (BD Bioscience) using FACSDiva software version 5.0.3. Quantifications were performed using Flowing software 2.5.1 (by Perttu Terho in collaboration with Turku Bioimaging).

ACKNOWLEDGEMENTS

We thank Louise von Stechow, Jordi Carreras Puigvert and Ram Sidappa for sharing experimental knowledge and assistance with spotting siRNAs.

REFERENCES

1. Acs,K., Luijsterburg,M.S., Ackermann,L., Salomons,F.A., Hoppe,T., and Dantuma,N.P. (2011). The AAA-ATPase VCP/p97 promotes 53BP1 recruitment by removing L3MBTL1 from DNA double-strand breaks. Nat. Struct. Mol. Biol. 18, 1345-1350.
2. Ayrapetov,M.K., Gursoy-Yuzugullu,O., Xu,C., Xu,Y., and Price,B.D. (2014). DNA double-strand breaks promote methylation of histone H3 on lysine 9 and transient formation of repressive chromatin. Proc. Natl. Acad. Sci. U. S. A 111, 9169-9174.
3. Bannister,A.J., Zegerman,P., Partridge,J.F., Miska,E.A., Thomas,J.O., Allshire,R.C., and Kouzarides,T. (2001). Selective recognition of methylated lysine 9 on histone H3 by the HP1 chromo domain. Nature 410, 120-124.
4. Bekker-Jensen,S. and Mailand,N. (2010). Assembly and function of DNA double-strand break repair foci in mammalian cells. DNA Repair (Amst) 9, 1219-1228.
5. Bennardo,N., Cheng,A., Huang,N., and Stark,J.M. (2008). Alternative-NHEJ is a mechanistically distinct pathway of mammalian chromosome break repair. PLoS. Genet. 4, e1000110.
6. Botuyan,M.V., Lee,J., Ward,I.M., Kim,J.E., Thompson,J.R., Chen,J., and Mer,G. (2006). Structural basis for the methylation state-specific recognition of histone H4-K20 by 53BP1 and Crb2 in DNA repair. Cell 127, 1361-1373.
7. Chapman,J.R., Taylor,M.R., and Boulton,S.J. (2012). Playing the end game: DNA double-strand break repair pathway choice. Mol. Cell 47, 497-510.
8. Chase,K.A. and Sharma,R.P. (2013). Nicotine induces chromatin remodelling through decreases in the methyltransferases GLP, G9a, Setdb1 and levels of H3K9me2. Int. J. Neuropsychopharmacol. 16, 1129-1138.
9. Chen,L., Li,Z., Zwolinska,A.K., Smith,M.A., Cross,B., Koomen,J., Yuan,Z.M., Jenuwein,T., Marine,J.C., Wright,K.L., and Chen,J. (2010). MDM2 recruitment of lysine methyltransferases regulates p53 transcriptional output. EMBO J. 29, 2538-2552.
10. Chou,D.M., Adamson,B., Dephoure,N.E., Tan,X., Nottke,A.C., Hurov,K.E., Gygi,S.P., Colaiacovo,M.P., and Elledge,S.J. (2010). A chromatin localization screen reveals poly (ADP ribose)-regulated recruitment of the repressive polycomb and NuRD complexes to sites of DNA damage. Proc. Natl. Acad. Sci. U. S. A 107, 18475-18480.
11. Cook,P.J., Ju,B.G., Telese,F., Wang,X., Glass,C.K., and Rosenfeld,M.G. (2009). Tyrosine dephosphorylation of H2AX modulates apoptosis and survival decisions. Nature 458, 591-596.
12. Doil,C., Mailand,N., Bekker-Jensen,S., Menard,P., Larsen,D.H., Pepperkok,R., Ellenberg,J., Panier,S., Durocher,D., Bartek,J., Lukas,J., and Lukas,C. (2009). RNF168 binds and amplifies ubiquitin conjugates on damaged chromosomes to allow accumulation of repair proteins. Cell 136, 435-446.
13 Epsztejn-Litman,S., Feldman,N., Abu-Remaileh,M., Shufaro,Y., Gerson,A., Ueda,J., Deplus,R., Fuks,F., Shinkai,Y., Cedar,H., and Bergman,Y. (2008). De novo DNA methylation promoted by G9a prevents reprogramming of embryonically silenced genes. Nat. Struct. Mol. Biol. 15, 1176-1183.
14. Fradet-Turcotte,A., Canny,M.D., Escribano-Diaz,C., Orthwein,A., Leung,C.C., Huang,H., Landry,M.C., Kitevski-LeBlanc,J., Noordermeer,S.M., Sicheri,F., and Durocher,D. (2013). 53BP1 is a reader of the DNA-damage-induced H2A Lys 15 ubiquitin mark. Nature 499, 50-54.
15. Fritsch,L., Robin,P., Mathieu,J.R., Souidi,M., Hinaux,H., Rougeulle,C., Harel-Bellan,A., Ameyar-Zazoua,M., and Ait-Si-Ali,S. (2010). A subset of the histone H3 lysine 9 methyltransferases Suv39h1, G9a, GLP, and SETDB1 participate in a multimeric complex. Mol. Cell 37, 46-56.
16. Gatti,M., Pinato,S., Maspero,E., Soffientini,P., Polo,S., and Penengo,L. (2012). A novel ubiquitin mark at the N-terminal tail of histone H2As targeted by RNF168 ubiquitin ligase. Cell Cycle 11, 2538-2544.
17. Guan,X., Zhong,X., Men,W., Gong,S., Zhang,L., and Han,Y. (2014). Analysis of EHMT1 expression and its correlations with clinical significance in esophageal squamous cell cancer. Mol. Clin. Oncol. 2, 76-80.
18. Helfricht,A., Wiegant,W.W., Thijssen,P.E., Vertegaal,A.C., Luijsterburg,M.S., and van Attikum,.H. (2013). Remodeling and spacing factor 1 (RSF1) deposits centromere proteins at DNA double-strand breaks to promote non-homologous end-joining. Cell Cycle 12, 3070-3082.
19. Hsiao,K.Y. and Mizzen,C.A. (2013). Histone H4 deacetylation facilitates 53BP1 DNA damage signaling and double-strand break repair. J. Mol. Cell Biol. 5, 157-165.
20. Hu,Y., Wang,C., Huang,K., Xia,F., Parvin,J.D., and Mondal,N. (2014). Regulation of 53BP1 protein stability by RNF8 and RNF168 is important for efficient DNA double-strand break repair. PLoS. One. 9, e110522.
21. Huang,J., Dorsey,J., Chuikov,S., Perez-Burgos,L., Zhang,X., Jenuwein,T., Reinberg,D., and Berger,S.L. (2010). G9a and Glp methylate lysine 373 in the tumor suppressor p53. J. Biol. Chem. 285, 9636-9641.
22. Huen,M.S., Grant,R., Manke,I., Minn,K., Yu,X., Yaffe,M.B., and Chen,J. (2007). RNF8 transduces the DNA-damage signal via histone ubiquitylation and checkpoint protein assembly. Cell 131, 901-914.
23. Huen,M.S., Sy,S.M., van Deursen,J.M., and Chen,J. (2008). Direct interaction between SET8 and proliferating cell nuclear antigen couples H4-K20 methylation with DNA replication. J. Biol. Chem. 283, 11073-11077.
24. Hurov,K.E., Cotta-Ramusino,C., and Elledge,S.J. (2010). A genetic screen identifies the Triple T complex required for DNA damage signaling and ATM and ATR stability. Genes Dev. 24, 1939-1950.

25. Kaidi,A. and Jackson,S.P. (2013). KAT5 tyrosine phosphorylation couples chromatin sensing to ATM signalling. Nature 498, 70-74.
26. Kalousi,A., Hoffbeck,A.S., Selemenakis,P.N., Pinder,J., Savage,K.I., Khanna,K.K., Brino,L., Dellaire,G., Gorgoulis,V.G., and Soutoglou,E. (2015). The Nuclear Oncogene SET Controls DNA Repair by KAP1 and HP1 Retention to Chromatin. Cell Rep. 11, 149-163.
27. Khosravi,R., Maya,R., Gottlieb,T., Oren,M., Shiloh,Y., and Shkedy,D. (1999). Rapid ATM-dependent phosphorylation of MDM2 precedes p53 accumulation in response to DNA damage. Proc. Natl. Acad. Sci. U. S. A 96, 14973-14977.
28. Khurana,S., Kruhlak,M.J., Kim,J., Tran,A.D., Liu,J., Nyswaner,K., Shi,L., Jailwala,P., Sung,M.H., Hakim,O., and Oberdoerffer,P. (2014). A macrohistone variant links dynamic chromatin compaction to BRCA1-dependent genome maintenance. Cell Rep. 8, 1049-1062.
29. Kleefstra,T., Kramer,J.M., Neveling,K., Willemsen,M.H., Koemans,T.S., Vissers,L.E., Wissink-Lindhout,W., Fenckova,M., van den Akker,W.M., Kasri,N.N., Nillesen,W.M., Prescott,T., Clark,R.D., Devriendt,K., van,R.J., de Brouwer,A.P., Gilissen,C., Zhou,H., Brunner,H.G., Veltman,J.A., Schenck,A., and van,B.H. (2012). Disruption of an EHMT1-associated chromatin-modification module causes intellectual disability. Am. J. Hum. Genet. 91, 73-82.
30. Kleefstra,T., Nillesen,W.M., and Yntema,H.G. (1993). Kleefstra Syndrome.
31. Kolas,N.K., Chapman,J.R., Nakada,S., Ylanko,J., Chahwan,R., Sweeney,F.D., Panier,S., Mendez,M., Wildenhain,J., Thomson,T.M., Pelletier,L., Jackson,S.P., and Durocher,D. (2007). Orchestration of the DNA-damage response by the RNF8 ubiquitin ligase. Science 318, 1637-1640.
32. Kondo,Y., Shen,L., Ahmed,S., Boumber,Y., Sekido,Y., Haddad,B.R., and Issa,J.P. (2008). Downregulation of histone H3 lysine 9 methyltransferase G9a induces centrosome disruption and chromosome instability in cancer cells. PLoS. One. 3, e2037.
33. Kramer,J.M., Kochinke,K., Oortveld,M.A., Marks,H., Kramer,D., de Jong,E.K., Asztalos,Z., Westwood,J.T., Stunnenberg,H.G., Sokolowski,M.B., Keleman,K., Zhou,H., van,B.H., and Schenck,A. (2011). Epigenetic regulation of learning and memory by Drosophila EHMT/G9a. PLoS. Biol. 9, e1000569.
34. Krishnan,N., Jeong,D.G., Jung,S.K., Ryu,S.E., Xiao,A., Allis,C.D., Kim,S.J., and Tonks,N.K. (2009). Dephosphorylation of the C-terminal tyrosyl residue of the DNA damage-related histone H2A.X is mediated by the protein phosphatase eyes absent. J. Biol. Chem. 284, 16066-16070.
35. Kwon,S.J., Park,J.H., Park,E.J., Lee,S.A., Lee,H.S., Kang,S.W., and Kwon,J. (2015). ATM-mediated phosphorylation of the chromatin remodeling enzyme BRG1 modulates DNA double-strand break repair. Oncogene 34, 303-313.
36. Lachner,M., O'Carroll,D., Rea,S., Mechtler,K., and Jenuwein,T. (2001). Methylation of histone H3 lysine 9 creates a binding site for HP1 proteins. Nature 410, 116-120.
37. Lee,J., Thompson,J.R., Botuyan,M.V., and Mer,G. (2008). Distinct binding modes specify the recognition of methylated histones H3K4 and H4K20 by JMJD2A-tudor. Nat. Struct. Mol. Biol. 15, 109-111.
38. Lee,Y.H., Kuo,C.Y., Stark,J.M., Shih,H.M., and Ann,D.K. (2013). HP1 promotes tumor suppressor BRCA1 functions during the DNA damage response. Nucleic Acids Res. 41, 5784-5798.
39. Luijsterburg,M.S., Acs,K., Ackermann,L., Wiegant,W.W., Bekker-Jensen,S., Larsen,D.H., Khanna,K.K., van Attikum,H., Mailand,N., and Dantuma,N.P. (2012). A new non-catalytic role for ubiquitin ligase RNF8 in unfolding higher-order chromatin structure. EMBO J. 31, 2511-2527.
40. Lukas,J., Lukas,C., and Bartek,J. (2011). More than just a focus: The chromatin response to DNA damage and its role in genome integrity maintenance. Nat. Cell Biol. 13, 1161-1169.
41. Mailand,N., Bekker-Jensen,S., Faustrup,H., Melander,F., Bartek,J., Lukas,C., and Lukas,J. (2007). RNF8 ubiquitylates histones at DNA double-strand breaks and promotes assembly of repair proteins. Cell 131, 887-900.
42. Mallette,F.A., Mattiroli,F., Cui,G., Young,L.C., Hendzel,M.J., Mer,G., Sixma,T.K., and Richard,S. (2012). RNF8- and RNF168-dependent degradation of KDM4A/JMJD2A triggers 53BP1 recruitment to DNA damage sites. EMBO J. 31, 1865-1878.
43. Matic,I., Schimmel,J., Hendriks,I.A., van Santen,M.A., van de Rijke,F., van,D.H., Gnad,F., Mann,M., and Vertegaal,A.C. (2010). Site-specific identification of SUMO-2 targets in cells reveals an inverted SUMOylation motif and a hydrophobic cluster SUMOylation motif. Mol. Cell 39, 641-652.
44. Matsuoka,S., Ballif,B.A., Smogorzewska,A., McDonald,E.R., III, Hurov,K.E., Luo,J., Bakalarski,C.E., Zhao,Z., Solimini,N., Lerenthal,Y., Shiloh,Y., Gygi,S.P., and Elledge,S.J. (2007). ATM and ATR substrate analysis reveals extensive protein networks responsive to DNA damage. Science 316, 1160-1166.
45. Meerang,M., Ritz,D., Paliwal,S., Garajova,Z., Bosshard,M., Mailand,N., Janscak,P., Hubscher,U., Meyer,H., and Ramadan,K. (2011). The ubiquitin-selective segregase VCP/p97 orchestrates the response to DNA double-strand breaks. Nat. Cell Biol. 13, 1376-1382.
46. Miller,K.M., Tjeertes,J.V., Coates,J., Legube,G., Polo,S.E., Britton,S., and Jackson,S.P. (2010). Human HDAC1 and HDAC2 function in the DNA-damage response to promote DNA nonhomologous end-joining. Nat. Struct. Mol. Biol. 17, 1144-1151.
47. Min,J., Allali-Hassani,A., Nady,N., Qi,C., Ouyang,H., Liu,Y., MacKenzie,F., Vedadi,M., and Arrowsmith,C.H. (2007). L3MBTL1 recognition of mono- and dimethylated histones. Nat. Struct. Mol. Biol. 14, 1229-1230.
48. Moore,K.E., Carlson,S.M., Camp,N.D., Cheung,P., James,R.G., Chua,K.F., Wolf-Yadlin,A., and Gozani,O. (2013). A general

molecular affinity strategy for global detection and proteomic analysis of lysine methylation. Mol. Cell 50, 444-456.
49. Nillesen,W.M., Yntema,H.G., Moscarda,M., Verbeek,N.E., Wilson,L.C., Cowan,F., Schepens,M., Raas-Rothschild,A., Gafni-Weinstein,O., Zollino,M., Vijzelaar,R., Neri,G., Nelen,M., Bokhoven,H., Giltay,J., and Kleefstra,T. (2011). Characterization of a novel transcript of the EHMT1 gene reveals important diagnostic implications for Kleefstra syndrome. Hum. Mutat. 32, 853-859.
50. Oda,H., Hubner,M.R., Beck,D.B., Vermeulen,M., Hurwitz,J., Spector,D.L., and Reinberg,D. (2010). Regulation of the histone H4 monomethylase PR-Set7 by CRL4(Cdt2)-mediated PCNA-dependent degradation during DNA damage. Mol. Cell 40, 364-376.
51. Panier,S., Ichijima,Y., Fradet-Turcotte,A., Leung,C.C., Kaustov,L., Arrowsmith,C.H., and Durocher,D. (2012). Tandem protein interaction modules organize the ubiquitin-dependent response to DNA double-strand breaks. Mol. Cell 47, 383-395.
52. Paulsen,R.D., Soni,D.V., Wollman,R., Hahn,A.T., Yee,M.C., Guan,A., Hesley,J.A., Miller,S.C., Cromwell,E.F., Solow-Cordero,D.E., Meyer,T., and Cimprich,K.A. (2009). A genome-wide siRNA screen reveals diverse cellular processes and pathways that mediate genome stability. Mol. Cell 35, 228-239.
53. Pei,H., Zhang,L., Luo,K., Qin,Y., Chesi,M., Fei,F., Bergsagel,P.L., Wang,L., You,Z., and Lou,Z. (2011). MMSET regulates histone H4K20 methylation and 53BP1 accumulation at DNA damage sites. Nature 470, 124-128.
54. Pierce,A.J. and Jasin,M. (2014). Measuring recombination proficiency in mouse embryonic stem cells. Methods Mol. Biol. 1105, 481-495.
55. Pierce,A.J., Johnson,R.D., Thompson,L.H., and Jasin,M. (1999). XRCC3 promotes homology-directed repair of DNA damage in mammalian cells. Genes Dev. 13, 2633-2638.
56. Rice,J.C., Briggs,S.D., Ueberheide,B., Barber,C.M., Shabanowitz,J., Hunt,D.F., Shinkai,Y., and Allis,C.D. (2003). Histone methyltransferases direct different degrees of methylation to define distinct chromatin domains. Mol. Cell 12, 1591-1598.
57. Roy,R., Chun,J., and Powell,S.N. (2012). BRCA1 and BRCA2: different roles in a common pathway of genome protection. Nat. Rev. Cancer 12, 68-78.
58. Shanbhag,N.M., Rafalska-Metcalf,I.U., Balane-Bolivar,C., Janicki,S.M., and Greenberg,R.A. (2010). ATM-dependent chromatin changes silence transcription in cis to DNA double-strand breaks. Cell 141, 970-981.
59. Shinkai,Y. and Tachibana,M. (2011). H3K9 methyltransferase G9a and the related molecule GLP. Genes Dev. 25, 781-788.
60. Smeenk,G., Wiegant,W.W., Marteijn,J.A., Luijsterburg,M.S., Sroczynski,N., Costelloe,T., Romeijn,R.J., Pastink,A., Mailand,N., Vermeulen,W., and van,A.H. (2013). Poly(ADP-ribosyl)ation links the chromatin remodeler SMARCA5/SNF2H to RNF168-dependent DNA damage signaling. J. Cell Sci. 126, 889-903.
61. Stewart,G.S., Panier,S., Townsend,K., Al-Hakim,A.K., Kolas,N.K., Miller,E.S., Nakada,S., Ylanko,J., Olivarius,S., Mendez,M., Oldreive,C., Wildenhain,J., Tagliaferro,A., Pelletier,L., Taubenheim,N., Durandy,A., Byrd,P.J., Stankovic,T., Taylor,A.M., and Durocher,D. (2009). The RIDDLE syndrome protein mediates a ubiquitin-dependent signaling cascade at sites of DNA damage. Cell 136, 420-434.
62. Stucki,M., Clapperton,J.A., Mohammad,D., Yaffe,M.B., Smerdon,S.J., and Jackson,S.P. (2005). MDC1 directly binds phosphorylated histone H2AX to regulate cellular responses to DNA double-strand breaks. Cell 123, 1213-1226.
63. Sun,Y., Jiang,X., Xu,Y., Ayrapetov,M.K., Moreau,L.A., Whetstine,J.R., and Price,B.D. (2009). Histone H3 methylation links DNA damage detection to activation of the tumour suppressor Tip60. Nat. Cell Biol. 11, 1376-1382.
64. Tachibana,M., Matsumura,Y., Fukuda,M., Kimura,H., and Shinkai,Y. (2008). G9a/GLP complexes independently mediate H3K9 and DNA methylation to silence transcription. EMBO J. 27, 2681-2690.
65. Tachibana,M., Sugimoto,K., Nozaki,M., Ueda,J., Ohta,T., Ohki,M., Fukuda,M., Takeda,N., Niida,H., Kato,H., and Shinkai,Y. (2002). G9a histone methyltransferase plays a dominant role in euchromatic histone H3 lysine 9 methylation and is essential for early embryogenesis. Genes Dev. 16, 1779-1791.
66. Tachibana,M., Ueda,J., Fukuda,M., Takeda,N., Ohta,T., Iwanari,H., Sakihama,T., Kodama,T., Hamakubo,T., and Shinkai,Y. (2005). Histone methyltransferases G9a and GLP form heteromeric complexes and are both crucial for methylation of euchromatin at H3-K9. Genes Dev. 19, 815-826.
67. Tang,J., Cho,N.W., Cui,G., Manion,E.M., Shanbhag,N.M., Botuyan,M.V., Mer,G., and Greenberg,R.A. (2013). Acetylation limits 53BP1 association with damaged chromatin to promote homologous recombination. Nat. Struct. Mol. Biol. 20, 317-325.
68. Typas,D., Luijsterburg,M.S., Wiegant,W.W., Diakatou,M., Helfricht,A., Thijssen,P.E., van de Broek,B., Mullenders,L.H., and van,A.H. (2015). The de-ubiquitylating enzymes USP26 and USP37 regulate homologous recombination by counteracting RAP80. Nucleic Acids Res.
68. Ueda,J., Tachibana,M., Ikura,T., and Shinkai,Y. (2006). Zinc finger protein Wiz links G9a/GLP histone methyltransferases to the co-repressor molecule CtBP. J. Biol. Chem. 281, 20120-20128.
69. Weil,D., Garcon,L., Harper,M., Dumenil,D., Dautry,F., and Kress,M. (2002). Targeting the kinesin Eg5 to monitor siRNA transfection in mammalian cells. Biotechniques 33, 1244-1248.
70. Weinstock,D.M., Nakanishi,K., Helgadottir,H.R., and Jasin,M. (2006). Assaying double-strand break repair pathway choice in mammalian cells using a targeted endonuclease or the RAG recombinase. Methods Enzymol. 409, 524-540.
71. Xiao,A., Li,H., Shechter,D., Ahn,S.H., Fabrizio,L.A., Erdjument-Bromage,H., Ishibe-Murakami,S., Wang,B., Tempst,P., Hofmann,K., Patel,D.J., Elledge,S.J., and Allis,C.D. (2009). WSTF regulates the H2A.X DNA damage response via a novel tyrosine

kinase activity. Nature 457, 57-62.
72. Zgheib,O., Pataky,K., Brugger,J., and Halazonetis,T.D. (2009). An oligomerized 53BP1 tudor domain suffices for recognition of DNA double-strand breaks. Mol. Cell Biol. 29, 1050-1058.

SUPPLEMENTAL INFORMATION

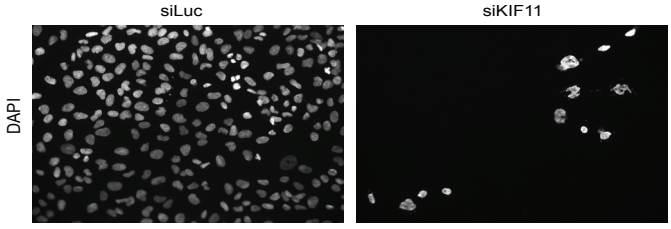

Figure S1. Knockdown efficiency confirmed with KIF11 knockdown. U2OS cells were reversely transfected with the indicated siRNAs and fixed after 3 days of cultivation. DNA was stained with DAPI to indicate cell nuclei, images were taken and the percentage of surviving cells in control and siKIF11 treated cells was estimated to 10%.

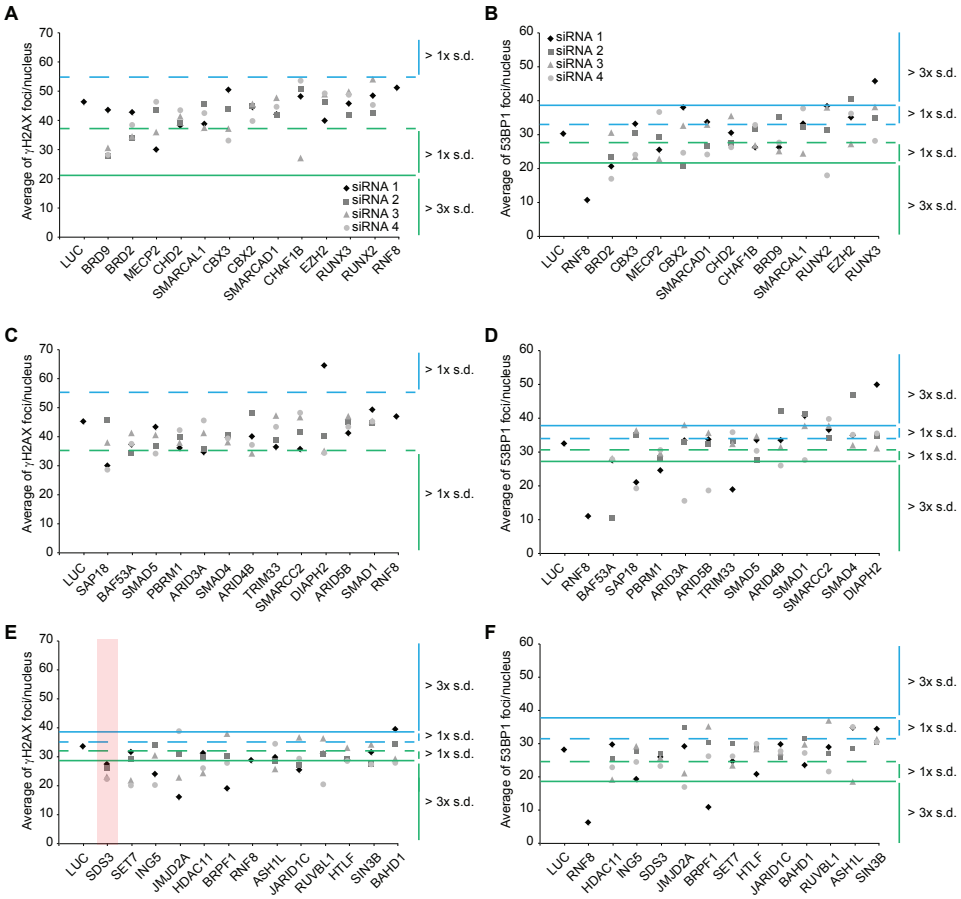

Figure S2. RNAi validation screen for novel regulators of γH2AX and 53BP1. Presented are the results from secondary validation screen, where four individual siRNAs per target were used to validate another 36 hits from primary screen (see first 12 hits in Fig. 1. D and E). Shown is the average number of γH2AX (A,C and E) and 53BP1 (B,D and F) foci/nucleus per siRNA per target from duplicate experiments. One and three times the standard deviation (s.d.) of the Luciferase control are indicated by dashed and continuous horizontal lines, respectively, in blue for an increase and in green for a decrease in average foci number/nucleus. Confirmed hits are indicated in red where at least 3 out of 4 siRNAs caused a change in average foci number/nucleus larger than three times the s.d. of Luciferase.

```
EHMT1_human MAAAD-AEAVPARGEPQQDCCVKTELLGEETPMAADEGSAEKQAGEAHMAADGETNGSCE 59
Ehmt1_mouse MAAADAEQAVLAKQETKQDCCMKTELLREDTPMAADEGSTEKQEGETPMAADGETNGSCE 60
            *****  :** *: * :****:***** *:**********:*** **: ************

EHMT1_human NSDASSHANAAKHTQDSARVNPQDGTNTLTRIAENGVSERDSEAAKQNHVTADDFVQTSV 119
Ehmt1_mouse KSGDPSHLNAPKHTQENTRASPQEGTNRVSRVAENGVSERDTEVGKQNHVTADDFMQTSV 120
            :*   ** ** ****:.:*..**:*** ::*:*********:*..**********:****

EHMT1_human IGSNGYILNKPALQAQPLRTTSTLASSLPGHAAKTLPGGAGKGRTPSAFPQTPAAPPATL 179
Ehmt1_mouse IGSNGYFLNKPALQGQPLRTPNILTSSLPGHAAKTLPGGASKCRTLSALPQTPTTAPTVP 180
            ******:*******.***** . *:***************.* ** **:****:: *:.

EHMT1_human GEGSADTEDRKLPAPGADVKVHRARKTMPKSVVGLHAASKDPREVREARDHKEPKEEINK 239
Ehmt1_mouse GEGSADTEDRKPTASGTDVRVHRARKTMPKSILGLHAASKDHREV---QDHKEPKEDINR 237
            ***********  * *:**:***********::******** ***   :*******:**:

EHMT1_human NISDFGRQQLLPPFPSLHQSLPQNQCYMATTKSQTACLPFVLAAAVSRKKKRRMGTYSLV 299
Ehmt1_mouse NISECGRQQLLPTFPALHQSLPQNQCYMATTKSQTACLPFVLAAAVSRKKKRRMGTYSLV 297
            ***: ******* **:**********************************************

EHMT1_human PKKKTKVLKQRTVIEMFKSITHSTVGSKGEKDLGASSLHVNGESLEMDSDEDDSEELEED 359
Ehmt1_mouse PKKKTKVLKQRTVIEMFKSITHSTVGAKGEKALDDSALHVNGESLEMDSEDEDSDELEDD 357
            **************************:**** *  *:************:::**:***:*

EHMT1_human DGHGAEQAAAFPTEDSRTSKESMSEADRAQKMDGESEEEQESVDTGEEEEGGDESDLSSE 419
Ehmt1_mouse EDHGAEQAAAFPTEDSRTSKESMSETDRAAKMDGDSEEEQESPDTGEDEDGGDESDLSSE 417
            : ************************:*** ****:******* ****:*:**********

EHMT1_human SSIKKKFLKRKGKTDSPWIKPARKRRRRSRKKPSGALGSESYKSSAGSAEQTAPGDSTGY 479
Ehmt1_mouse SSIKKKFLKRRGKTDSPWIKPARKRRRRSRKKPSSMLGSEACKSSPGSMEQAALGDSAGY 477
            **********:************************. ****: *** ** **:* ***:**

EHMT1_human MEVSLDSLDLRVKGILSSQA--EGLANGPDVLETDGLQEVPLCSCRMETPKSREITTLAN 537
Ehmt1_mouse MEVSLDSLDLRVRGILSSQTENEGLASGPDVLGTDGLQEVPLCSCRMETPKSREISTLAN 537
            ************:******:  ****.***** **********************:****

EHMT1_human NQCMATESVDHELGRCTNSVVKYELMRPSNKAPLLVLCEDHRGRMVKHQCCPGCGYFCTA 597
Ehmt1_mouse NQCMATESVDHELGRCTNSVVKYELMRPSNKAPLLVLCEDHRGRMVKHQCCPGCGYFCTA 597
            ************************************************************

EHMT1_human GNFMECQPESSISHRFHKDCASRVNNASYCPHCGEESSKAKEVTIAKADTTSTVTPVPGQ 657
Ehmt1_mouse GNFMECQPESSISHRFHKDCASRVNNASYCPHCGEEASKAKEVTIAKADTTSTVTLAPGQ 657
            ************************************:****************** .***

EHMT1_human EKGSALEGRADTTTGSAAGPPLSEDDKLQGAASHVPEGFDPTGPAGLGRPTPGLSQGPGK 717
Ehmt1_mouse EKSLAAEGRADTTTGSIAGAPED--ERSQSTAPQAPECFDPAGPAGLVRPTSGLSQGPGK 715
            **. * ********** ** * .  :: *.:* :.** ***:***** *** ********

EHMT1_human ETLESALIALDSEKPKKLRFHPKQLYFSARQGELQKVLLMLVDGIDPNFKMEHQNKRSPL 777
Ehmt1_mouse ETLESALIALDSEKPKKLRFHPKQLYFSARQGELQKVLLMLVDGIDPNFKMEHQSKRSPL 775
            ************************************************.*****

EHMT1_human HAAAEAGHVDICHMLVQAGANIDTCSEDQRTPLMEAAENNHLEAVKYLIKAGALVDPKDA 837
Ehmt1_mouse HAAAEAGHVDICHMLVQAGANIDTCSEDQRTPLMEAAENNHLDAVKYLIKAGAQVDPKDA 835
            ******************************************:********** ******

EHMT1_human EGSTCLHLAAKKGHYEVVQYLLSNGQMDVNCQDDGGWTPMIWATEYKHVDLVKLLLSKGS 897
Ehmt1_mouse EGSTCLHLAAKKGHYDVVQYLLSNGQMDVNCQDDGGWTPMIWATEYKHVELVKLLLSKGS 895
            ***************:**********************************:**********

EHMT1_human DINIRDNEENICLHWAAFSGCVDIAEILLAAKCDLHAVNIHGDSPLHIAARENRYDCVVL 957
Ehmt1_mouse DINIRDNEENICLHWAAFSGCVDIAEILLAAKCDLHAVNIHGDSPLHIAARENRYDCVVL 955
            ************************************************************

EHMT1_human FLSRDSDVTLKNKEGETPLQCASLNSQVWSALQMSKALQDSAPDRPSPVERIVSRDIARG 1017
Ehmt1_mouse FLSRDSDVTLKNKEGETPLQCASLSSQVWSALQMSKALRDSAPDKPVAVEKTVSRDIARG 1015
            ************************.**************:*****:*  **: ********
```

```
EHMT1_human YERIPIPCVNAVDSEPCPSNYKYVSQNCVTSPMNIDRNITHLQYCVCIDDCSSSNCMCGQ 1077
Ehmt1_mouse YERIPIPCVNAVDSELCPTNYKYVSQNCVTSPMNIDRNITHLQYCVCVDDCSSSTCMCGQ 1075
            *************** **:****************************:******.*****

EHMT1_human LSMRCWYDKDGRLLPEFNMAEPPLIFECNHACSCWRNCRNRVVQNGLRARLQLYRTRDMG 1137
Ehmt1_mouse LSMRCWYDKDGRLLPEFNMAEPPLIFECNHACSCWRNCRNRVVQNGLRARLQLYRTQDMG 1135
            ************************************************************:***

EHMT1_human WGVRSLQDIPPGTFVCEYVGELISDSEADVREEDSYLFDLDNKDGEVYCIDARFYGNVSR 1197
Ehmt1_mouse WGVRSLQDIPLGTFVCEYVGELISDSEADVREEDSYLFDLDNKDGEVYCIDARFYGNVSR 1195
            ********** ************************************************

EHMT1_human FINHHCEPNLVPVRVFMAHQDLRFPRIAFFSTRLIEAGEQLGFDYGERFWDIKGKLFSCR 1257
Ehmt1_mouse FINHHCEPNLVPVRVFMSHQDLRFPRIAFFSTRLIQAGEQLGFDYGERFWDVKGKLFSCR 1255
            *****************:*****************:***************:********

EHMT1_human CGSPKCRHSSAALAQRQASAAQEAQEDGLPDTSSAAAADPL                    1298
Ehmt1_mouse CGSSKCRHSSAALAQRQASAAQEPQENGLPDTSSAAAADPL                    1296
            *** ******************* **:**************
```

Figure S3. EHMT1 protein sequence is quiet conserved between mouse and human.
Entries Q9H9B1 for human EHMT1 and Q5DW34 for mouse Ehmt1 were aligned using the Uniprot alignment tool available at www.uniprot.org. The conserved amino acids are indicated by a green asterisk.

Table S1. List of siRNA screen gene targets and results. (A) List of 227 gene targets and positive (siLUC) and negative (siRNF8) controls. Indicated are gene symbols, Gene IDs, Accession numbers and the obtained Z-scores calculated from the average amount of γH2AX or 53BP1 foci determined during the first siRNA screen. Blue indicates an increase and green a decrease in the average foci number/nucleus. Gray specifies the validation selected targets. (B) List of 48 target genes against which four single siRNAs were employed during the deconvolution screen. Depicted are gene symbols and the average number of foci/ nucleus for γH2AX and 53BP1. Hit results are indicated in red, when minimal 3 out of 4 siRNAs caused an increase (blue) or decrease (green) larger than three times the standard deviation of the control Luciferase.

A

nr.	siRNA SMARTpools	Gene ID	Accession Number	Z-score gH2AX foci	Z-score 53BP1 foci
1	AOF2	23028	NM_015013	-0,052	-0,616
2	ARID1A	8289	NM_006015	-0,307	1,159
3	ARID1B	57492	NM_017519	-	-
4	ARID2	196528	NM_152641	-	-
5	ARID3A	1820	NM_005224	2,348	4,968
6	ARID3B	10620	NM_006465	0,860	3,039
7	ARID4A	8841	NM_003883	-	-
8	ARID4B	51742	NM_016374	-12,181	-0,234
9	ARID5A	10865	NM_212481	0,649	0,171
10	ARID5B	84159	NM_032199	0,341	-4,214
11	ASH1L	55870	NM_018489	-2,329	6,283
12	ATAD2	29028	NM_014109	0,135	0,910
13	ATRX	546	NM_000489	0,517	0,647
14	BAIAP3	57597	XM_371084	-	-
15	BAP18	86	NM_004301	0,638	-6,061
16	BAHD1	22893	NM_014952	-1,196	4,796
17	BAZ1A	11177	NM_013448	-0,145	8,129
18	BAZ1B	9031	NM_032408	-1,548	8,691
19	BAZ2A	11176	NM_013449	-0,425	9,938
20	BAZ2B	29994	NM_013450	0,356	0,221
21	BMI1	648	NM_005180	-	-
22	BPTF	2186	NM_182641	-	-
23	BRD1	23774	NM_014577	-	-
24	BRD2	6046	NM_001113182	2,160	-4,732
25	BRD3	8019	NM_007371	-0,041	6,962
26	BRD4	23476	NM_014299	-	-
27	BRD7	29117	NM_013263	-	-
28	BRD8	10902	NM_006696	-4,647	-5,215
29	BRD9	65980	NM_023924	0,517	7,887
30	BRDT	676	NM_207189	-	-
31	BRPF1	7862	NM_001003694	0,712	5,265
32	BRPF3	27154	NM_015695	0,139	-4,728
33	BRWD1	54014	NM_033656	0,303	8,359
34	BRWD3	254065	NM_153252	0,327	8,959
35	BTG1	694	NM_00173	-	-
36	BTG2	7832	NM_006763	0,315	-1,104
37	BTG3	10950	NM_001130914	-0,293	-3,307
38	BTG4	54766	NM_017589	0,064	-1,299
39	CARM1	10498	NM_199141	0,681	1,614
40	CBX1	10951	NM_006807	-	-
41	CBX2	84733	NM_032647	-0,329	3,398
42	CBX3	11335	NM_007276	0,883	3,916
43	CBX4	8535	NM_003655	-	-
44	CBX5	23468	NM_001127321	7,771	2,163
45	CBX6	23466	NM_014292	0,407	6,409
46	CBX7	23492	NM_175709	1,191	9,059
47	CBX8	57332	NM_020649	-	-
48	CECR2	27443	NM_031413	1,233	2,287
49	CHC1	1104	NM_001269	-	-
50	CHAF1B	8208	NM_005441	1,492	2,167
51	CHD1	1105	NM_001270	0,085	8,161
52	CHD1L	9557	NM_004284	-	-
53	CHD2	1106	NM_001271	-0,232	7,103
54	CHD3	1107	NM_001005273	0,164	4,039
55	CHD5	26038	NM_015557	-	-
56	CHD6	84181	NM_032221	-	-
57	CHD7	55636	XM_098762	-	-
58	CHD8	57680	NM_020920	0,340	5,956
59	CHD9	80205	NM_025134	1,430	10,656
60	CREBBP	1387	NM_001079846	-	-
61	DIAPH1	1729	NM_001079812	-	-
62	DIAPH2	1730	NM_006729	-23,710	-1,904
63	DNAJC1	64215	NM_022365	-	-
64	DNAJC2	27000	NM_001129887	-1,546	-1,509
65	DNMT1	1786	NM_001379	-0,036	1,320
66	DNMT2	1787	NM_004412	1,935	-1,001
67	DNMT3B	1789	NM_006892	-2,630	0,894
68	DNMT3L	29947	NM_013369	-	-
69	DMAP1	55929	NM_019100	-	-
70	DOT1L	84444	NM_032482	-3,333	2,056
71	EHMT1	79813	NM_024757	-0,352	4,070
72	EHMT2	10919	NM_006709	0,580	3,274
73	EID1	23741	NM_014335	-	-
74	EID2	163126	NM_153232	-0,710	0,280
75	EID2B	126272	NM_152361	-	-
76	EID3	49386	NM_001008394	-	-
77	EP300	2033	NM_001429	-	-
78	EP400	57634	NM_015409	-1,165	-1,402
79	EPC1	80314	NM_025209	0,499	1,839
80	EPC2	26122	NM_015630	-	-
81	ERCC6	2074	NM_000124	-	-
82	ERCC6L	54821	NM_017669	0,243	0,914
83	ERCC6L2	375748	NM_001010895	0,847	1,765
84	EZH1	2145	NM_001991	-	-
85	EZH2	2146	NM_004456	0,378	2,211
86	GAS41	8089	NM_006530	-3,792	-1,997
87	HZAFZ	3015	NM_002106	0,145	-0,589
88	HDAC1	3065	NM_004964	-	-
89	HDAC2	3066	NM_001527	-	-
90	HDAC3	8841	NM_003883	-0,913	0,360
91	HDAC4	9757	NM_006037	0,657	8,444
92	HDAC5	10014	NM_001015053	-	-
93	HDAC6	10013	NM_006044	0,390	4,665
94	HDAC7	51564	NM_001098416	-	-
95	HDAC8	55869	NM_018486	-	-
96	HDAC9	9734	NM_014707	-	-
97	HDAC10	83933	NM_032019	-	-
98	HDAC11	79885	NM_001136041	0,416	5,562
99	HELLS	3070	NM_018063	0,669	1,859
100	HLTF	6596	NM_003071	0,812	2,104
101	HTATIP	10524	NM_006388	0,025	6,982
102	ING1	3621	NM_198217	0,664	0,888
103	ING2	3622	NM_001564	-	-
104	ING3	54556	NM_019071	-	-
105	ING5	84289	NM_032329	0,238	2,097
106	JARID1A	5927	NM_001042603	-	-
107	JARID1B	10765	NM_006618	0,099	1,086
108	JARID1C	8242	NM_004187	1,144	6,477
109	JARID1D	8284	NM_004653	-	-
110	JARID2	3720	NM_004973	-	-
111	JMJD1A	55818	NM_018433	-0,656	-1,535
112	JMJD1B	51780	NM_016604	-	-

B

nr.	single siRNAs	Average nr. of gH2AX foci	Average nr. of 53BP1 foci
1	ARID3A-1	34,709	33,431
	ARID3A-2	35,872	32,983
	ARID3A-3	41,308	38,000
	ARID3A-4	45,607	15,583
2	ARID4B-1	40,113	33,527
	ARID4B-2	48,029	42,216
	ARID4B-3	34,248	31,498
	ARID4B-4	37,187	26,017
3	ARID5B-1	41,248	33,742
	ARID5B-2	45,036	32,307
	ARID5B-3	47,079	35,690
	ARID5B-4	43,398	18,636
4	ASH1L-1	29,857	34,797
	ASH1L-2	28,510	28,637
	ASH1L-3	25,773	18,578
	ASH1L-4	34,499	35,024
5	BAF53A-1	37,320	27,618
	BAF53A-2	34,337	10,598
	BAF53A-3	41,310	28,172
	BAF53A-4	37,566	27,899
6	BAHD1-1	39,551	23,547
	BAHD1-2	34,254	31,420
	BAHD1-3	29,322	29,740
	BAHD1-4	27,907	27,183
7	BAZ1A-1	44,008	37,954
	BAZ1A-2	46,402	49,354
	BAZ1A-3	37,175	36,031
	BAZ1A-4	41,249	32,503
8	BAZ1B-1	48,752	46,987
	BAZ1B-2	43,338	32,860
	BAZ1B-3	48,881	53,982
	BAZ1B-4	49,071	32,026
9	BAZ2A-1	43,911	37,987
	BAZ2A-2	46,865	39,910
	BAZ2A-3	48,140	41,062
	BAZ2A-4	38,701	36,868
10	BRD2-1	42,750	20,686
	BRD2-2	34,069	23,351
	BRD2-3	34,466	30,597
	BRD2-4	38,406	17,000
11	BRD9-1	43,541	38,397
	BRD9-2	27,618	35,081
	BRD9-3	30,567	25,157
	BRD9-4	28,137	27,653
12	BRPF1-1	19,121	10,885
	BRPF1-2	30,179	30,455
	BRPF1-3	37,980	35,169
	BRPF1-4	27,873	26,217
13	BRWD1-1	47,821	37,626
	BRWD1-2	49,041	48,068
	BRWD1-3	46,082	42,087
	BRWD1-4	54,512	55,835
14	BRWD3-1	37,748	35,885
	BRWD3-2	46,638	39,317
	BRWD3-3	46,486	35,114
	BRWD3-4	48,968	42,493
15	CBX2-1	44,519	38,029
	CBX2-2	44,928	20,631
	CBX2-3	45,643	32,665
	CBX2-4	39,741	24,657
16	CBX3-1	50,434	33,197
	CBX3-2	43,752	30,588
	CBX3-3	37,122	23,478
	CBX3-4	33,044	24,081
17	CBX5-1	48,271	38,292
	CBX5-2	41,808	38,217
	CBX5-3	44,553	38,157
	CBX5-4	50,795	47,493
18	CHAF1B-1	48,149	33,236
	CHAF1B-2	50,627	31,618
	CHAF1B-3	27,068	26,824
	CHAF1B-4	53,529	32,853
19	CHD2-1	38,172	30,544
	CHD2-2	39,159	27,515
	CHD2-3	41,335	35,504
	CHD2-4	43,432	26,287
20	DIAPH2-1	64,573	49,936
	DIAPH2-2	40,234	34,614
	DIAPH2-3	35,143	31,135
	DIAPH2-4	34,391	35,518
21	EHMT1-1	45,574	48,228
	EHMT1-2	48,704	46,018
	EHMT1-3	46,625	43,123
	EHMT1-4	44,315	32,989
22	EHMT2-1	39,674	37,355
	EHMT2-2	37,511	32,100
	EHMT2-3	47,576	43,129
	EHMT2-4	41,884	36,700
23	EZH2-1	39,880	29,526
	EZH2-2	46,136	40,425
	EZH2-3	48,924	27,246
	EZH2-4	49,208	36,206
24	HDAC11-1	31,271	29,743
	HDAC11-2	29,731	25,594
	HDAC11-3	24,397	19,157
	HDAC11-4	26,088	22,879
25	HTLF-1	28,987	20,826
	HTLF-2	29,363	28,703
	HTLF-3	33,097	28,346
	HTLF-4	28,550	29,955
26	ING5-1	24,078	19,351
	ING5-2	34,031	27,771
	ING5-3	30,486	29,216
	ING5-4	20,234	24,502
27	JARID1C-1	25,482	29,813
	JARID1C-2	27,112	25,785
	JARID1C-3	36,700	27,412
	JARID1C-4	29,350	27,726
28	JMJD2A-1	16,118	29,191
	JMJD2A-2	31,051	34,878
	JMJD2A-3	22,855	21,087
	JMJD2A-4	38,854	16,947

113	JMJD1C	221037	NM_004241	-	-
114	JMJD2A	9682	NM_014663	0,053	2,317
115	JMJD2B	23030	NM_015015	-	-
116	JMJD2C	23081	NM_015061	-	-
117	JMJD2D	55693	NM_018039	-	-
118	JMJD3	23135	NM_001080424	0,144	-0,616
119	JMJD4	65094	NM_023007	-	-
120	JMJD5	79831	NM_024773	-	-
121	KAT2A	2648	NM_021078	-	-
122	KAT2B	8850	NM_003884	-	-
123	LRCH4	4034	NM_002319	0,369	1,860
124	Luciferase			-0,024	0,188
125	LOC33012			-	-
126	MBD1	4152	NM_002384	-	-
127	MBD2	8932	NM_003927	-8,576	-1,711
128	MBD3	53615	NM_003926	-	-
129	MBD4	8930	NM_003925	-	-
130	MBD5	55777	NM_018328	-	-
131	MBD6	114785	NM_052897	-14,592	0,393
132	MEAF6	64769	NM_022756	-0,084	-0,593
133	MECP2	4204	NM_001110792	6,108	0,646
134	METTL5	29081	NM_014168	-0,181	-0,030
135	MLL	4297	NM_005933	-	-
136	MLL2	8085	NM_003482	-	-
137	MLL3	58508	NM_170606	-	-
138	MLL4	9757	NM_014727	-	-
139	MLL5	55904	NM_018682	-	-
140	MORF4	10933	NM_006791	-1,942	-0,272
141	MORF4L1	10934	NM_006792	-12,662	2,971
142	MSL3	10943	NM_006800	-	-
143	MYBL2	4605	NM_002466	-	-
144	MYSM1	114803	NM_001085487	-	-
145	MYST1	84148	NM_032188	-	-
146	MYST2	11143	NM_007067	7,458	2,752
147	MYST3	7994	NM_006766	10,389	2,813
148	MYST4	23522	NM_012330	-	-
149	NCOR1	9611	NM_006311	0,357	0,593
150	NCOR2	9612	NM_006312	-	-
151	OR11H2	79334	NM_001197287	2,360	0,601
152	PBRM1	55193	NM_018165	0,661	-5,779
153	PCGF1	84759	NM_032673	-0,116	-0,822
154	PCGF2	7703	NM_007144	-	-
155	PCGF3	10336	NM_006315	-	-
156	PCGF5	84333	NM_032373	0,228	-0,011
157	PCGF6	84108	NM_001011663	-	-
158	PHF19	26147	NM_001009936	-	-
159	PTDSR	23210	NM_015167	-	-
160	RAD21	5885	NM_006265	0,721	0,601
161	RAD54B	25788	NM_012415	1,193	1,645
162	RAD54L	8438	NM_003579	0,885	1,652
163	RCOR1	23186	NM_015156	-	-
164	RCOR2	283248	NM_173587	-1,438	0,010
165	RCOR3	55758	NM_018254	0,429	1,679
166	RERE	473	NM_001042681	-	-
167	RNF8	9025	NM_003958	0,720	-25,492
168	RNF2	6045	NM_007212	-	-
169	RUNX2	860	NM_001015051	-2,247	-0,661
170	RUNX3	864	NM_001031680	-0,328	2,131
171	RUVBL1	8607	NM_003707	-4,117	-1,698
172	RUVBL2	10856	NM_006666	-	-
173	SAP18	10284	NM_005870	-19,393	-0,976
174	SAP30	8819	NM_003864	0,298	0,421
175	SCML2	10389	NM_006089	-	-
176	SDS3	64426	NM_022491	-3,815	-0,325
177	SET7	80854	NM_030648	-	- *
178	SETD1A	9739	NM_014712	0,491	0,437
179	SETD1B	23067	NM_015048	-1,258	-0,511
180	SETD2	29072	NM_014159	-0,812	-0,383
181	SETD4	54093	NM_017438	0,456	-1,283
182	SETD7	80854	NM_030648	-1,982	0,777
183	SETDB	387893	NM_020382	-	-
184	SHPRH	257218	NM_173082	0,377	-0,089
185	SIN3A	25942	NM_015477	-	-
186	SIN3B	23309	NM_015260	3,442	4,329
187	SMAD1	4086	NM_001003688	1,946	4,277
188	SMAD2	4087	NM_001003652	-	-
189	SMAD3	4088	NM_005902	-	-
190	SMAD4	4089	NM_005359	0,926	2,254
191	SMAD5	4090	NM_001001419	-4,744	-3,551
192	SMAD6	4091	NM_005585	-	-
193	SMAD7	4092	NM_005904	-	-
194	SMAD9	4093	NM_001127217	-	-
195	SMARCA1	6594	NM_003069	-	-
196	SMARCA2	6595	NM_003070	-	-
197	SMARCA4	6597	NM_001128844	-2,566	-1,001
198	SMARCA5	8467	NM_003601	-6,963	-0,911
199	SMARCAD1	56916	NM_020159	1,213	2,067
200	SMARCAL1	50485	NM_001127207	3,213	0,074
201	SMARCC1	6599	NM_003074	-	-
202	SMARCC2	6601	NM_001130420	-0,559	3,506
203	SMC1A	8243	NM_006306	-	-
204	SMURF1	57154	NM_020429	-	-
205	SMURF2	64750	NM_022739	-	-
206	SMYD1	150572	NM_198274	-	-
207	SMYD2	56950	NM_020197	-8,556	-0,848
208	SMYD3	64754	NM_022743	-	-
209	SMYD4	114826	NM_052928	-	-
210	SMYD5	10322	NM_006062	-	-
211	SP100	6672	NM_003113	-0,587	4,373
212	SP110	3431	NM_080424	-	-
213	SP140L	93349	NM_138402	-1,378	0,070
214	SUPT7L	9913	NM_014860	-	-
215	SUV39H1	6839	NM_003173	-	-
216	SUV39H2	79723	NM_024670	-	-
217	TADA2A	6871	NM_001488	1,094	1,783
218	TADA2B	93624	NM_152293	-	-
219	TAF1	6872	NM_004606	1,425	5,945
220	TAF3	83860	NM_031923	-	-
221	TAF8	129685	NM_138572	1,287	8,499
222	TERF1	7013	NM_017489	0,168	1,330
223	TERF2	7014	NM_005652	0,831	1,565
224	TRIM28	10155	NM_005762	-	-
225	TRIM33	51592	NM_015906	0,437	7,458
226	TRIM66	9866	XM_084529	-	-
227	TRRAP	8295	NM_003496	-2,941	1,017
228	VPS72	6944	NM_005997	1,563	1,852
229	ZZZ3	26009	NM_015534	-	-

29	MECP2-1	29,996	25,534
	MECP2-2	43,504	29,313
	MECP2-3	35,965	22,877
	MECP2-4	46,336	36,664
30	MYST2-1	38,398	34,566
	MYST2-2	40,433	41,936
	MYST2-3	48,390	47,312
	MYST2-4	58,962	56,949
31	MYST3-1	47,404	41,053
	MYST3-2	43,238	36,808
	MYST3-3	42,828	34,410
	MYST3-4	50,200	44,705
32	PBRM1-1	36,131	24,594
	PBRM1-2	39,934	28,288
	PBRM1-3	37,933	29,673
	PBRM1-4	42,264	30,588
33	RUNX2-1	48,417	45,783
	RUNX2-2	42,341	31,484
	RUNX2-3	54,035	38,037
	RUNX2-4	45,251	18,002
34	RUNX3-1	45,730	32,427
	RUNX3-2	41,724	34,769
	RUNX3-3	49,802	38,162
	RUNX3-4	48,719	28,175
35	RUVBL1-1	31,084	28,982
	RUVBL1-2	30,966	27,084
	RUVBL1-3	36,389	36,962
	RUVBL1-4	20,497	21,611
36	SAP18-1	30,051	21,053
	SAP18-2	45,632	35,004
	SAP18-3	38,001	36,388
	SAP18-4	28,637	19,251
37	SDS3-1	27,482	25,971
	SDS3-2	26,137	27,110
	SDS3-3	23,145	25,753
	SDS3-4	22,319	23,255
38	SET7-1	31,671	24,693
	SET7-2	29,397	30,115
	SET7-3	21,860	23,444
	SET7-4	20,093	26,192
39	SIN3B-1	31,613	34,431
	SIN3B-2	27,615	30,182
	SIN3B-3	34,242	31,382
	SIN3B-4	27,409	30,489
40	SMAD1-1	49,333	40,716
	SMAD1-2	44,636	41,325
	SMAD1-3	45,448	37,746
	SMAD1-4	45,260	27,640
41	SMAD4-1	39,672	34,932
	SMAD4-2	40,632	46,858
	SMAD4-3	38,128	32,007
	SMAD4-4	39,416	35,117
42	SMAD5-1	43,368	33,552
	SMAD5-2	36,655	27,726
	SMAD5-3	40,625	34,702
	SMAD5-4	34,178	30,364
43	SMARCA4-1	45,851	28,184
	SMARCA4-2	41,750	33,136
	SMARCA4-3	43,027	39,069
	SMARCA4-4	48,007	41,378
44	SMARCAD1-1	42,035	33,727
	SMARCAD1-2	41,820	26,656
	SMARCAD1-3	47,700	32,960
	SMARCAD1-4	44,607	24,154
45	SMARCAL1-1	38,758	35,131
	SMARCAL1-2	45,404	32,260
	SMARCAL1-3	37,424	24,474
	SMARCAL1-4	42,449	37,733
46	SMARCC2-1	35,750	36,560
	SMARCC2-2	41,507	34,079
	SMARCC2-3	46,748	37,802
	SMARCC2-4	48,262	39,778
47	SP100-1	43,653	39,158
	SP100-2	48,938	45,393
	SP100-3	44,175	38,094
	SP100-4	40,679	35,287
48	TRIM33-1	36,470	18,962
	TRIM33-2	38,833	33,239
	TRIM33-3	47,287	32,415
	TRIM33-4	43,421	35,873

Increase in average number of foci/nucleus
Decrease in average number of foci/nucleus
Hits selected for validation screen
Hit
* faultive selection